2005

Development of process techniques for bistable microbeam fabrication

Varsha Francis
Louisiana State University and Agricultural and Mechanical College

DEVELOPMENT OF PROCESS TECHNIQUES FOR BISTABLE MICROBEAM FABRICATION

A Thesis

Submitted to the Graduate Faculty of the
Louisiana State University and
Agricultural and Mechanical College
in partial fulfillment of the
requirements for the degree of
Master of Science in Electrical Engineering
in
The Department of Electrical and Computer Engineering

By
Varsha Francis
B.E, Osmania University, India, 2003
December, 2005

Acknowledgements

I would like to start by thanking my major professor, Dr. Martin Feldman for giving me this opportunity to study micro fabrication at LSU. He has been an excellent teacher and mentor during my graduate studies as he expertly guided me through my research endeavors. I would also like to thank Dr. Ashok Srivastava and Dr. Wei for being a part of my thesis committee.

I dedicate this work to my parents for their constant support and encouragement which has got me so far.

In addition I want to thank my fellow student Li Jiang for helping me in my initial stages at EMDL. I would also like to thank Dr.Ajmera and Dr. In-hyouk Song for their guidance and Mr. Golden Hwuang of the Electronic Material and Device Laboratory in the Electrical and Computer Engineering Department for his help in EMDL.

I would finally like to thank all the fellow students of Electronic Material and Device Laboratory for all their help, especially Bharath Thiruvengadachari for helping me with the Edwards Coating system and Satish Thiruvengadam with the AFM.

Table of Contents

List of Tables

List of Figures

List of Symbols

Symbol	Meaning
D_C	Distance moved by the cantilever beam (um)
D_B	Distance moved by the bistable beams (um)
D	Displacement of both cantilever and bistable beams when $D_C = D_B$ for the same beam length
D-space	Lattice spacing between (111) planes (in this case of nickel)
l	Bistable beam length (mm)
t	Thickness of the beam in consideration (um)
l_C	Cantilever beam length (mm)
n	Number of combs
g	Gap between the combs (um)
V	Voltage applied to the beam in being considered (V)
F	Force in the electrostatic combs
C	% Compression in the bistable beam of length l
f	Scaling factor

Abstract

A design which uses bistable beams to modulate light is suggested in this thesis and appropriate processing techniques are presented. A beam when placed under compression above the Euler limit has two stable states. The compression in an electroplated beam can be controlled by the plating current density of nickel during electrodeposition. This beam is attached to an electromechanical comb. Voltages applied to the combs cause the beam to snap from one stable state to another.

Structures were designed with dimensions that gave feasible voltages, snap distances, compressions required to snap. A two mask process was used for the fabrication of the device. The first mask delineates the sacrificial layer (AZ P4620) and the second mask delineates the electroplating mould (SU8-50). Developing techniques such as mechanical stirring at room temperature obtained bistable beam lengths of up to 1mm having an aspect ratio of 4. For higher aspect ratios such as 10 the amount of developed beam length was 200um. The dimensions that could be obtained were not adequate for practical applications.

Use of better equipment such as a mega sonic bath is suggested to improve the development in the bistable beam length. Reducing the bistable beam lengths is also suggested as an option.

1. Introduction

1.1 Background in MEMS

Cantilever beams are used in MEMS (acronym for Micro Electro Mechanical Systems) for a variety of well known applications such as sensors and actuators, accelerometers etc. The use of bistable beams for optical modulation of light is suggested here. The "bistable states" concept for light valves has been used before in the T.I. (Texas Instruments) micro-mirror array. An extension of the same concept has been suggested for the bistable beams. The first step to achieve this is presented in this thesis.

- **Transmission Light Valve Array**

  Light valve arrays are used to project images by separately controlling the light intensity at each pixel. To minimize blocking the light path, the electronics associated with the array has always been placed behind the array. The array is used in reflection, which complicates the projection system. This light valve array can be used in transmission.

- **Proposed Optical System**

  The moving (bistable) beams can be used as shutters in light valves (Figure 1a).

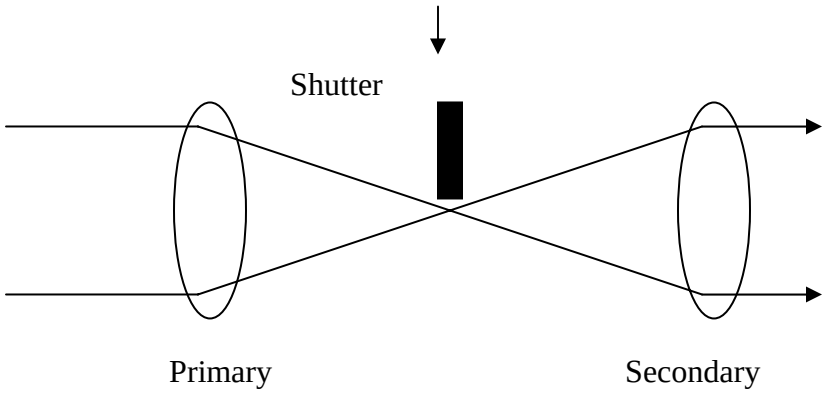

Figure 1a: A one to one telescope. The output contains all the light in the original beam, but it can be gated by a small portion of the shutter.

In the above figure a parallel beam of light is brought to a waist by a primary lens, and then re-collimated by a secondary lens. The shutter which blocks the light only needs to move a distance equal to the diameter of the waist. An array of such light valves may be used to generate an image (Figure 1b), with each valve acting as a pixel and each shutter controlling the light at that pixel.

The secondary lenses shown look the same with slightly smaller focal lengths, to minimize cross-talk, or light from one pixel entering a neighboring pixel. If the illumination entering each light valve is not collimated, the minimum diameter of the focused light will be increased; nevertheless the light will always be focused to a small fraction of the pixel area. The remaining area is available for the mechanical drive mechanism for the shutter, and the electronics and wiring associated with the pixel. It is precisely this factor which makes it possible for this light valve array to operate in transmission.

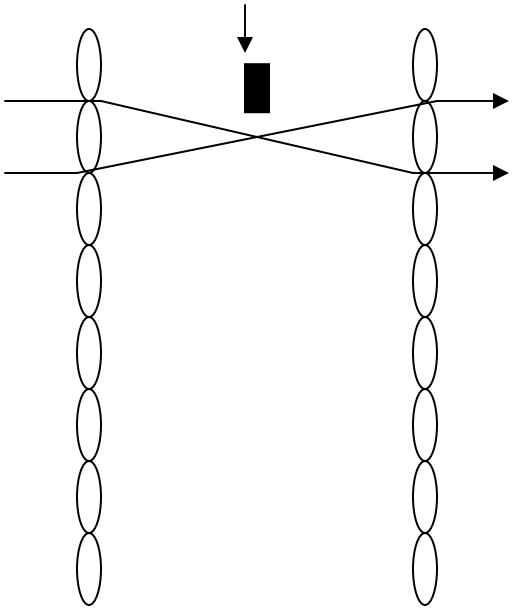

Figure 1b: An array of telescopes. Each element in the array has its own movable shutter which gates that individual element. For clarity, the light going through only one element is shown. If all the shutters are open, all of the input light goes through.

- **Comb Mechanism**

The shutter is driven by an electromechanical comb (Figure 2), a proposed mechanism for moving parts in MEMS. An unusual feature is that both ends of the moving central members are rigidly attached to stationary mounts. A small amount of compression is applied to the central member. This has two effects: (1) The force required for a given deflection is reduced, and (2) Two stable states are generated, with the central member curved either to the left or to the right. Voltages applied to the combs switch the central member between two states.

The amount of compression in the central member is a critical parameter: Too little compression and the member is stable, too much and the force required to switch between the two states increases.

The stress in electroplating may be controlled by the current density that is maintained during plating. Alternatively, stress may be controlled by the plating on a substrate that has been elastically deformed, and then releasing the substrate when the plating is completed.

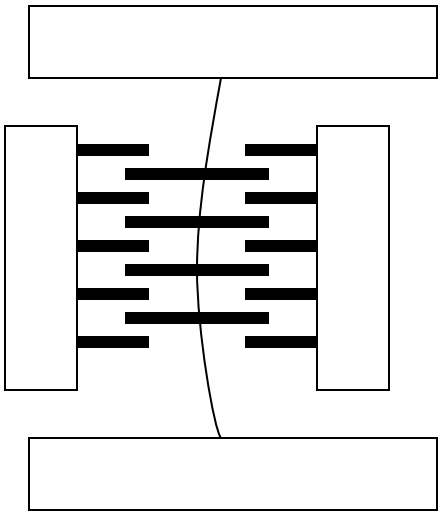

Figure 2: The bistable mechanical arrangement used to drive the shutter. The comb structures on either side repel the central member when a drive voltage is applied to them. The central member is shown bending to the left – it also has a stable configuration bending to the right. For clarity, the shutter itself has not been shown and the shape of the deflected beam has been simplified.

- **Word Lines and Bit Lines in the Mechanical Memory**

The shutter drive shown in Figure 2 may be arranged in an array and accessed by means of word lines and bit lines (Figure 3). Each bit line has two strings: one goes to the right handed comb and one goes to the left handed comb. These correspond to "set" and "reset" functions for the mechanical bistable memory. When the right hand string is at a voltage, +V, the left hand string is at 0. This is defined as setting the selected pixel to logic "1". Similarly, when the left hand string is at +V, the right hand string is at 0. This sets the selected pixel to logic "0".

Unselected word lines are held at voltage +1/2V. Thus, the absolute value of the voltage difference between both the left hand and the right hand combs and the center member is V/2. Since combs produce a repulsive force that is proportional to the square of the voltage across them, the resulting forces at an unselected word are proportional to $1/4V^2$. To the extent that the left hand and right hand combs produce equal forces, they cancel, and the net force at an unselected word is zero.

A selected word line may be held at 0 volts. This produces a repulsive force proportional to V^2 from the left comb for logic 0, and a similar repulsive force from the right comb for a logic1. There are no forces from the left comb for logic 1 or the right comb for logic 0. The operating margins are thus between an unbalanced force proportional to V^2 for writing a selected word, and two oppositely directed, and nominally equal, forces proportional to $1/4V^2$ for unselected words.

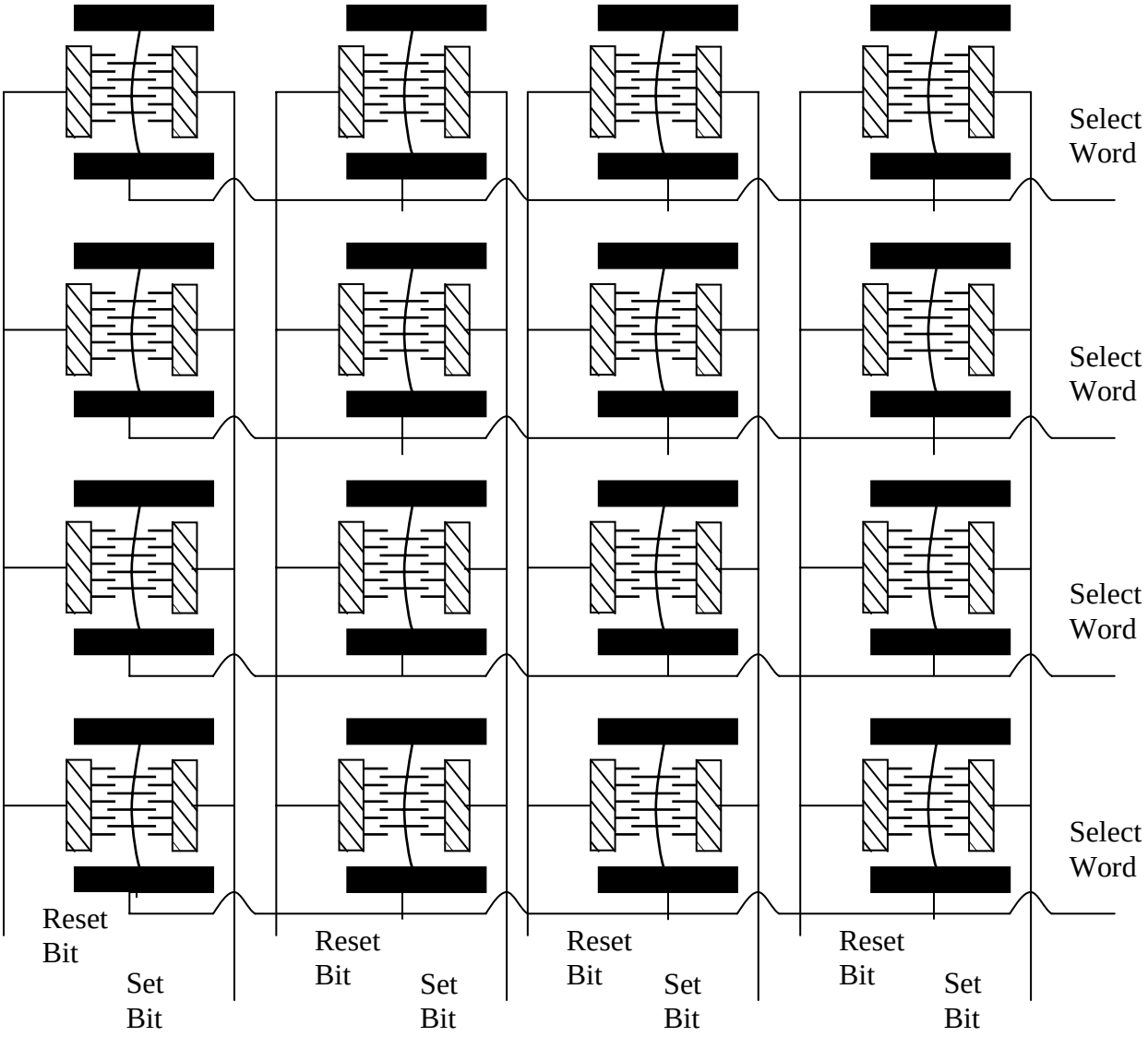

Figure 3: Word lines and bit lines for a two dimensional 4×4 array of shutters

A better choice is to select a word by returning the word line to -1/2V. This produces a repulsive force proportional to $9/4V^2$ from the left comb for logic 0, and a similar repulsive force from the right comb for logic 1. The repulsive forces from the left comb for logic 1 or the right comb for logic 0 are proportional to $1/4V^2$, or a net force proportional to $2V^2$ for writing a selected word. This increases the operating margin by a factor of 2 compared to returning the word lines to 0 volts.

1.2 Background in Fabrication

- **Processing**

The processing techniques, temperatures used, etc, vary in each of these stages depending on the type of photoresist used in MEMS. A general overview is discussed here. The flowchart in Figure 4 shows typical steps involved in the processing. A more detailed description of the steps actually developed is given in Chapter 3.

Wafer cleaning is a wafer preparation step followed by coating the desired resist on the wafer by spinning the wafer on a vacuum chuck. Each resist has its own spin cycle which again varies based on the thickness of the coating. The lower the thickness of the coating the higher the final spin speed required. Soft baking evaporates the solvent from the coated resist; this helps prevent damage to the mask used. The exposure for MEMS structures is normally done in the contact mode when an optical lithography system is used. When more than one level of resist is needed during processing, alignment marks are introduced into the masks to ensure proper alignment of the levels. The Post Exposure Bake is an optional stage if the resist is thinner than 10um. For chemically amplified layers this stage helps polymerize the resist through cationic photo amplification. For positive resist development dissolves the areas of the resist where bonds were broken during the exposure, thus giving rise to the desired pattern. Similarly, for negative resist development dissolves areas of the resist that were not cross linked during exposure. Hard baking is once again an optional step; it is done to strengthen the resist against any further energetic processes such as ion implantation and plasma etching. It also helps improve adhesion.
Structure patterning involves thin film deposition or etching (wet or dry) of materials. Removal of the excess resist is generally done unless the resist is required to be a part of the final device.

- **Sacrificial Layer**

MEMS fabrication requires the release of compliant mechanical structures. A sacrificial layer is typically used to provide a structural layer on which device layers can be deposited and subsequently removed to leave a suspended or freestanding device. There are several sacrificial layers commonly used in MEMS fabrication such as polyimide etc. Lately the use of photoresist as a sacrificial layer has been done. This saves a significant number of processing steps. Resist can also be removed without the inherent problem of residues or stiction from wet processing.

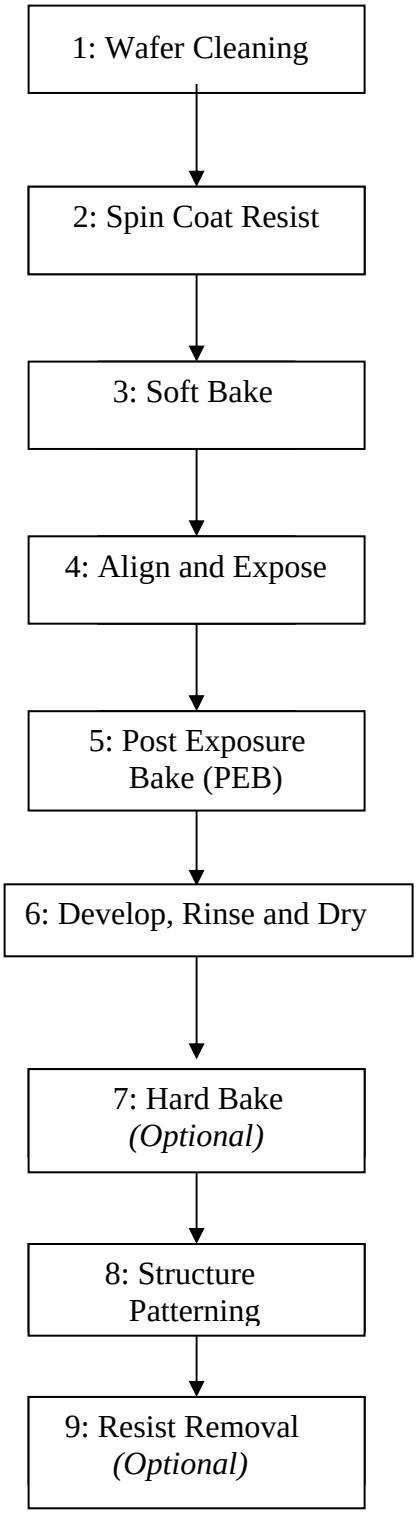

Figure 4: Sequence of general processing steps in MEMS fabrication.

1.3 Literature Review

The integration of MEMS with electronics has been done before in this department. This was a starting point for work with similar structures. Most previous MEMS structures were cantilever type [1]. The use of bistable MEMS with two stable working states would be the first of its kind. The fabrication technique adopted to make the device is as important as the design. The literature review aims at obtaining a simple and effective technique used for similar structures.

The use of photoresist as a sacrificial layer reduces the number of processing steps; this is a common practice in MEMS fabrication nowadays. It was used by many workers [3] and the improvements carried out on it by Song [2] proved particularly useful for the present case. In the previous work [2], suspended MEMS cantilever structures were designed using SU-8 as an electroplating mould. In addition to this photoresist was used for the sacrificial layer. The two mask process shown in Figure 5 was used to fabricate a cantilever free standing structure. The first mask delineated the sacrificial layer and the second mask, called the mould mask delineated the electroplating mould. First a photoresist was spun on the silicon substrate (S1813) and then patterned with the sacrificial layer mask (Figure 5(a)). After development the photoresist is baked for hardening at high temperatures to help prevent any kind of deterioration in the later stages of processing [2]. Metal layers were then sputtered to give an electroplating base layer (Fig 5(b)). A layer of SU-8 photoresist was then spun and patterned using the mould mask (Fig 5(c)). After the substrate was electroplated to deposit nickel only in the mould areas, the system was then stripped of the SU-8 mould. The metal layers were etched and the sacrificial layer was also stripped to leave the structure standing suspended and free to move (Fig 5(d)).

This concept was extended by using a glass substrate and using AZ P4620 instead of S1813. This was done to obtain a thicker sacrificial layer which could be etched and removed more easily at a later stage than a thinner one.

1.4 Goals of Research and Organization of Thesis

- **Goals of Research**

The goals for this research are:

1. To design bistable structures for the purposes mentioned in section 1.1.
2. To setup an electroplating apparatus to plate the structures and to study the plating characteristics.
3. To determine the processing parameters for development of the bistable beams in the available lab facilities and to determine if the dimensions are feasible.

The actual construction and testing of the bistable devices are beyond the scope of this thesis, but the tools are now in place so that this may be accomplished.

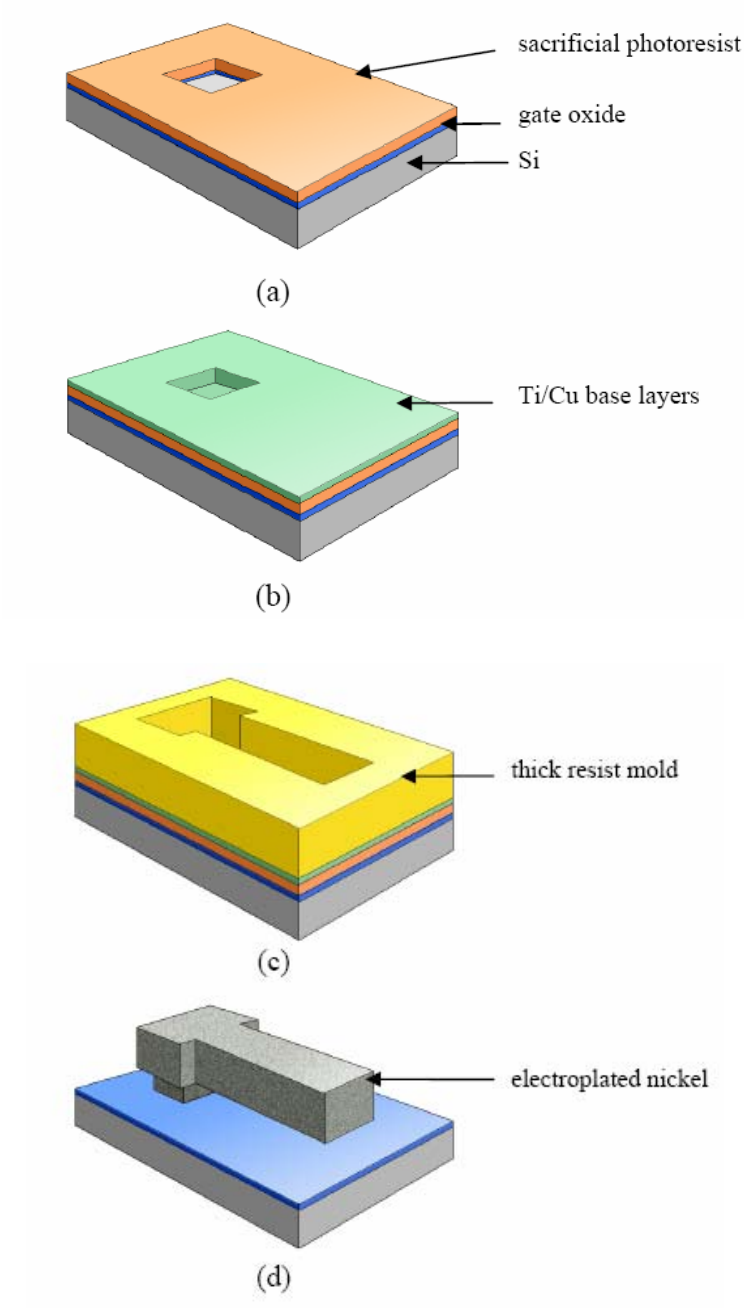

Figure 5: The two mask fabrication process adopted for the present case. (a) Patterning the photoresist sacrificial layer. (b) Coating Ti and Cu electroplating base metals. (c) Patterning resist as electroplating mould. (d) Suspended nickel structure after electroplating and etching off the electroplating mould and the base and the sacrificial layers. The Si substrate and SiO_2 gate oxide were replaced with just a SiO_2 substrate for the present case. Reprinted by permission. See Appendix A.1.

- **Organization of Thesis**

  This chapter (1) introduces the area in which this particular MEMS device can work, the processing steps involved and the literature review. Chapter 2 discusses the equations and concepts that led to the design of these structures. Chapter 3 describes the experimental setup and the lab conditions used. Chapter 4 presents the results achieved, the conclusions and also discusses the possible future work.

2. Design of the Structures

2.1 Derivation of the Euler Load

2.1.1 Euler Critical Load [6]

For a short column having a uniform cross sectional area A and subjected to an axial load P shown in Figure 6a, the stress intensity ρ induced on a beam section is, $\rho = \frac{P}{A}$

As the axial load increases at some point the beam compresses along its length and fails due to crushing. If P_C is the crushing load, then the crushing stress is, $\rho_C = P_C/A$.

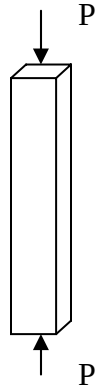

Figure 6a: A short column being subjected to an axial load P.

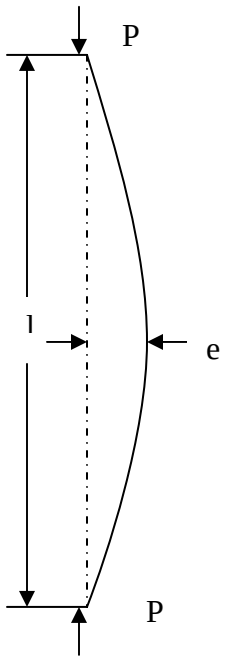

Figure 6b: A long column buckling due to an axial load P.

On the other hand, columns that are long do not fail by crushing but bend or buckle when their axial load reaches a certain critical value. This load at which the column buckles is called the Euler critical load. For these columns the buckling load is less than the crushing load, i.e., the long columns have a lower failure load than the short columns.

Hence the longer columns bend or buckle rather than crush. At this stage the system is said to be elastically unstable. Figure 6b shows an axially loaded column having a length l that has buckled due to the applied P.

2.1.2 Derivation of the Euler Critical Load for a Beam Fixed at Two Ends [6]

- **Deriving the equation for pure bending**

Theory of simple bending

Pure bending or simple bending is defined as the condition of the beam when it is absolutely free from shear and is subjected only to a bending moment. Figure 7a shows a part of a beam that has been subjected to pure bending. The part of length δx being subjected to bending has deformed as shown in Figure 7b. Some fibers in them elongate and some shorten whereas the otherwise remain the same. The layers where these fibers are neither elongated nor shortened is called the neutral layer or the neutral surface. The line of intersection of a neutral surface on a cross section is called the neutral axis (EF).

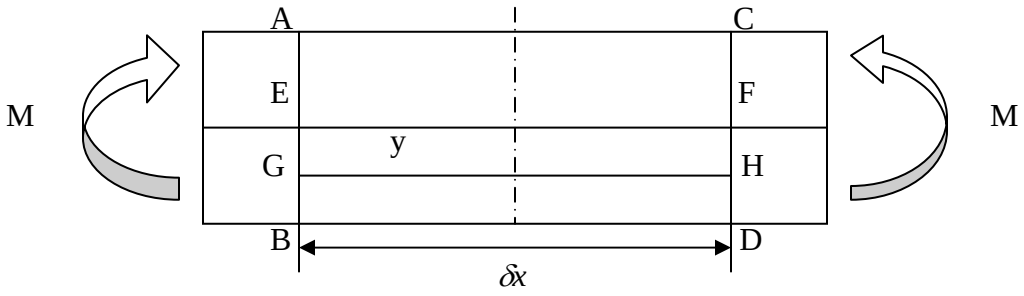

Figure 7a: A part of a long column subjected to pure bending.

Let A'B' and C'D' meet at O. Let the angle between A'B' and C'D' be θ. Let the radius of the neutral surface be R. Consider the fiber GH distant y from the neutral layer.

Therefore, change in length for GH = G'H'-GH = $((R+y).\theta) - R\theta = y.\theta$

Strain in GH = e = change in length/original length = $y\theta / R\theta = y/R$.

If the stress intensity in the fiber is f, then the strain is e = f/E.
where E is the Young's Modulus of the beam, defined by Hooke's law to be the stress in the beam divided by its strain.

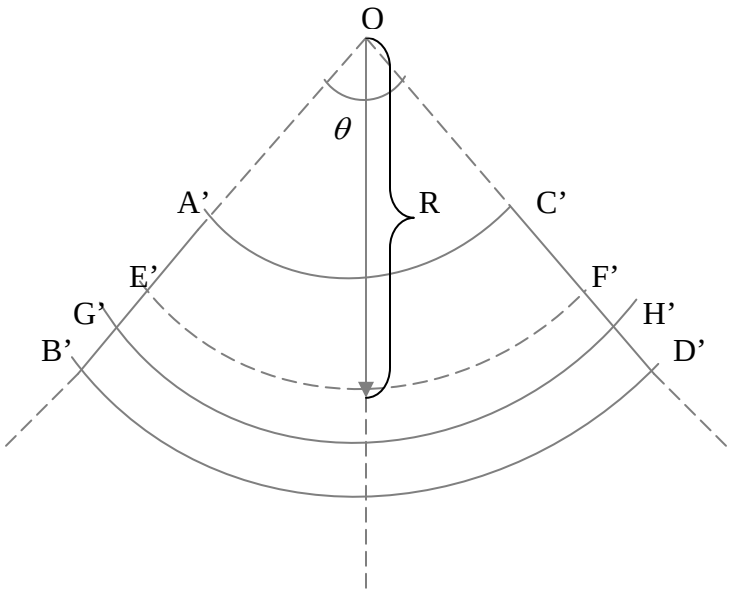

Figure 7b: Part of the long column that deformed due to bending**.**

Therefore,

e = f/E = y/R or f/y = E/R …… (1)

Moment of Resistance

The moment of resistance is two equal and opposite resistances acting at a point that form a couple. Consider a small elemental area δa at a distance y from the neutral axis of this cross section (Figure 8).
The Moment of resistance offered by the elemental area = moment of the thrust about the neutral axis = $\frac{E}{R} y^2 \delta a$
Therefore, the total moment of resistance offered by the beam section = M = $\frac{E}{R} \sum_{y_t}^{y_c} y^2 \delta a$

where, y_c is the distance from the neutral axis to the top of the beam and
y_t is the distance from the neutral axis to the bottom of the beam
as shown in Figure 8.

Since $\sum_{y_t}^{y_c} y^2 \delta a$ is the moment of inertia of the beam section about the central axis given by the standard notation of I.

Therefore $M = \frac{E}{R} I$ Hence, $\frac{M}{I} = \frac{E}{R}$ …… (2)

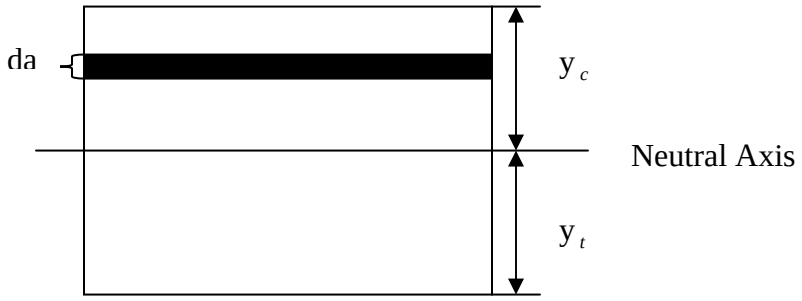

Figure 8: Cross section of the a long column showing an elemental area da.

Combining equation (1) and (2) we get,

$$\frac{M}{I} = \frac{f}{y} = \frac{E}{R} \quad \text{…… (3)}$$

This is called the bending equation or flexure formula.

- **Using the Pure Bending Equation to Derive Euler Critical Load for a Beam Fixed at Two Ends**

Figure 9 shows a column AB of length l whose ends A and B are both fixed. Therefore, there is a restraint moment say M_O at each end. Let P be the axial load.
The bending equation based on the theory of pure bending derived in the previous section is used,

$$\frac{M}{I} = \frac{f}{y} = \frac{E}{R}$$

where, M is the bending moment of the system
I is the moment of inertia
f is the stress intensity
y is the distance from the neutral axis
E is the Young's modulus of the beam
R is the radius of the neutral surface
Hence,

$$\frac{M}{I} = \frac{E}{R} \quad \therefore \quad M = \frac{EI}{R}$$

The bending moment M of the system is,

$$M = \sum M = -Py + M_O$$

Therefore,

$$-Py + M_O = \frac{EI}{R}$$

where, x and y are co-ordinates of a point on a curve. Here the distance x locates a point on the elastic curve of a deflected beam and y is the deflection of the same point from its initial position (as in Figure 9). However, the deflections tolerated in the vast majority of engineering structures are very small and so the slope dy/dx is negligible compared with unity.

$$\therefore \quad \frac{1}{R} \approx \frac{d^2y}{dx^2}$$

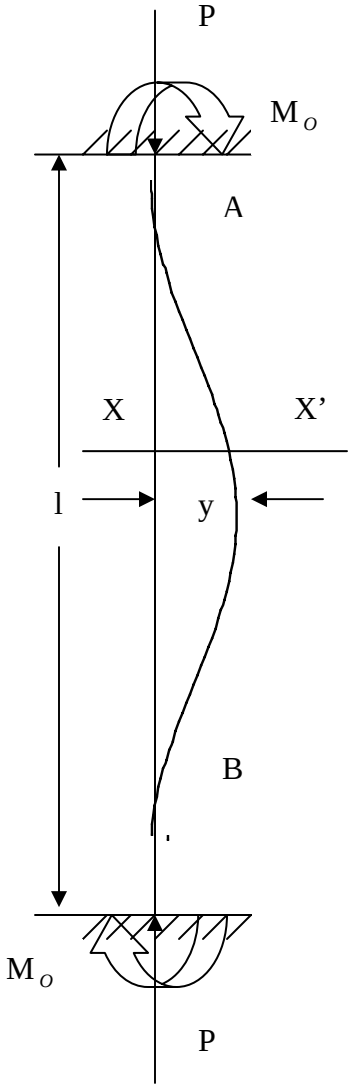

Figure 9: A beam fixed at both ends having a restraint moment M_O and an axial load P.

Hence, for a section XX' at a distance of x from the lower end B, the bending moment at a section XX' is given by,

$$EI\frac{d^2y}{dx^2} = M_O - Py$$

$$\therefore \qquad \mathrm{EI}\frac{\mathrm{d}^2y}{\mathrm{dx}^2} + Py = M_O$$

$$\therefore \qquad \frac{\mathrm{d}^2y}{\mathrm{dx}^2} + \frac{P}{EI}y = \frac{M_O}{EI}$$

The solution to the above differential equation is,

$$y = C_1\cos\left(x\sqrt{\frac{P}{EI}}\right) + C_2\sin\left(x\sqrt{\frac{P}{EI}}\right) + \frac{M_O}{P}$$

where, C_1 and C_2 are constants of integration. The slope at any section is given by,

$$\frac{dy}{dx} = -C_1\sqrt{\frac{P}{EI}}\sin\left(x\sqrt{\frac{P}{EI}}\right) + C_2\sqrt{\frac{P}{EI}}\cos\left(x\sqrt{\frac{P}{EI}}\right)$$

At B, the deflection is zero.
Therefore, at x = 0 and y = 0

$$0 = C_1 + \frac{M_O}{P} \quad \therefore \quad C_1 = -\frac{M_O}{P}$$

At B, the slope is zero,
Therefore at, x = 0, dy/dx = 0

$$0 = C_2\sqrt{\frac{P}{EI}} \quad \therefore \quad C_2 = 0$$

At A, the deflection is zero
Therefore at x = l, y = 0

$$0 = -\frac{M_O}{P}\cos\left(l\sqrt{\frac{P}{EI}}\right) + \frac{M_O}{P}$$

$$\therefore \qquad \frac{M_O}{P}\left[1 - \cos\left(l\sqrt{\frac{P}{EI}}\right)\right] = 0$$

$$\therefore \quad \cos\left(l\sqrt{\frac{P}{EI}}\right) = 1.$$

$$\therefore \quad \left(l\sqrt{\frac{P}{EI}}\right) = 0, 2\pi, 4\pi, 6\pi.....$$

Considering the first practical value,

$$l\sqrt{\frac{P}{EI}} = 2\pi$$

$$P = \frac{4\pi^2 EI}{l^2}$$

Hence, the Euler critical load for a beam fixed at both ends is

$$P = \frac{4\pi^2 EI}{l^2} \quad \text{……..……..……} \quad (4)$$

2.1.3 Calculation of Compression Required at the Euler Critical Load for Bistable Beams

The derivation of compression at Euler critical load was calculated below. Consider a rectangular beam as in Fig 10 of length denoted by l, width denoted by w and thickness denoted by t. When it is bent along its thickness, the moment of inertia in that plane is given by I,

$$\text{I} = \frac{w \times t^3}{12} \quad \text{……..……..} \quad (5)$$

The internal stress in the system is given by

$$\sigma = \frac{P}{A} \quad \text{……..……..} \quad (6)$$

where, σ is the internal stress (Newton*meter^{-2})
P is force at the Euler critical limit (Newton)
A is cross sectional area (meter^2)

By definition the Euler critical load for a beam fixed at both ends was derived in section 2.1.2 as,

$$P = \frac{4\pi^2 EI}{l^2} \quad \text{..... (7)}$$

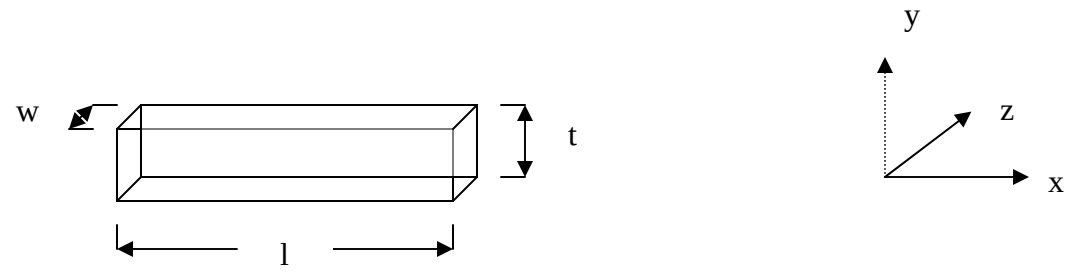

Figure 10: A rectangular beam having a length l, width w and thickness t.

where, E is Young's Modulus (Newton* meter^{-2})
l is length (length)
I is moment of inertia given by (5)

Substituting Equation 5 in Equation 7 we get

$$P = \frac{4\pi^2 Ewt^3}{12l^2} \quad \text{..... (8)}$$

Substituting Equation 8 in Equation 6 we get

$$\sigma = \frac{4\pi^2 Et^2}{12l^2} \quad \text{.....} \quad \text{(9)}$$

(Since, A = w.t)

From Hooke's law we know that

E = Stress/Strain

Hence

Strain at Euler's limit or the compression obtained at the Euler critical load is

$$dl/l = \sigma/E = \frac{4\pi^2 t^2}{12l^2}$$

$$dl/l = 3.29(t/l)^2 \quad \text{..... (10)}$$

When we operate in the region above the critical load the beam requires an external force to change its state.

2.2 Relevant Work Previously Done in the Department

2.2.1 Previous Work Done for Cantilever Beams

The electrostatic force of repulsion that exists in the comb is given by [9]

$$F = \frac{X\varepsilon ntV^2}{g} \quad \text{.. (11)}$$

where, X is the fringing coefficient which is equal to 1
ε is the permittivity
n is the number of comb fingers
t is the thickness of the beam (in um)
g is the gap between the comb fingers (in um)
V is the applied voltage (in volts)

Previous work [9] in our department has shown the motion, D (in nm) of a cantilever beam similar to those currently made in our department [1] by plating nickel in a LIGA like structure, is given by

$$D_C = \left(\frac{knV^2 l_C{}^3}{gt^3}\right) \times 10^{-3} \quad \text{.. (12)}$$

where, k is a constant equal to 2.0
n is the number of comb fingers
V is the voltage applied (in volts)
l_C is the length of the cantilever beam (in mm)
g is the gap (in um)
t is the thickness of the cantilever beams (in um)
D_C is the distance moved by the beam (in um)

We have some initial experimental results [9] with n=5, V=72V, l_C=1.8mm, g=10um and t=10um. Equation 2 predicts that the motion, D_C=15.1nm. What is actually observed is D_C=17nm.

There is a theoretical prediction [9] with n=20, V=50V, l_C=10 (or 20) mm, g=10um, t=10um. Equation 12 predicts that the motion, D_C=10 (or 80)um. What is predicted is D_C=8.4 (or 67.2) um. So Equation 12 predicts a little too low for the one case and a little too high for the other.

2.2.2 Previous Work Done in Nickel Plating

Earlier work [5] has shown that it's possible to control the stress in nickel plating by varying the plating current density. This stress also varies with the composition of the solution used and the pH of the solution. Figure 11 shows the relation between D-space in the plated nickel versus the plating current density for a nickel sulfate solution operated at

a pH of 3.5. D-space is the spacing between the (111) planes (for the nickel) obtained from X-ray diffraction measurements. The graph for stress in nickel can be derived from changes in D-space. This concept can be extended to other nickel plating solutions.

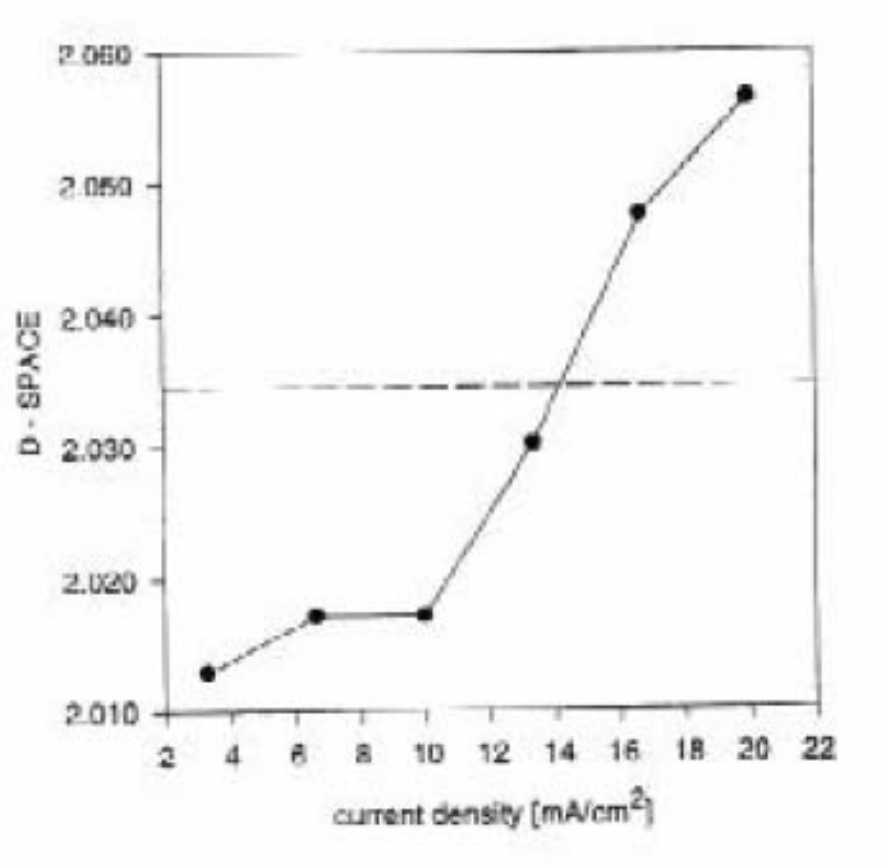

Figure 11: Spacing (D-space) between (111) planes for electroformed Ni as a function of plating current density. The dotted line represents the lattice spacing value expected from a stress-free layer. Reprinted by permission. See appendix A.2.

2.3 Derivation of Governing Equations to Design Bistable Structures

2.3.1 Model Experiments Done

- **Force versus Distance Moved Relations for Cantilever Structures**

  A model cantilever beam system was setup as shown in Figure 12. Standard hacksaw blades were used as beams. They were cut to different lengths ranging from 2” to 10”, having a thickness of 0.6mm and a width of 6.35mm. The force applied and the corresponding distance moved by the beam was tabulated for different beam lengths. Figure 13 shows the displacement versus force values of a cantilever beam plotted for a beam length of 7” and having a linear fit. Similar curves were obtained

for the other beam lengths also. This shows that the relation between force applied and the displacement for a cantilever beam is linear.

Figure 12: Cantilever beam showing displacement on application of force.

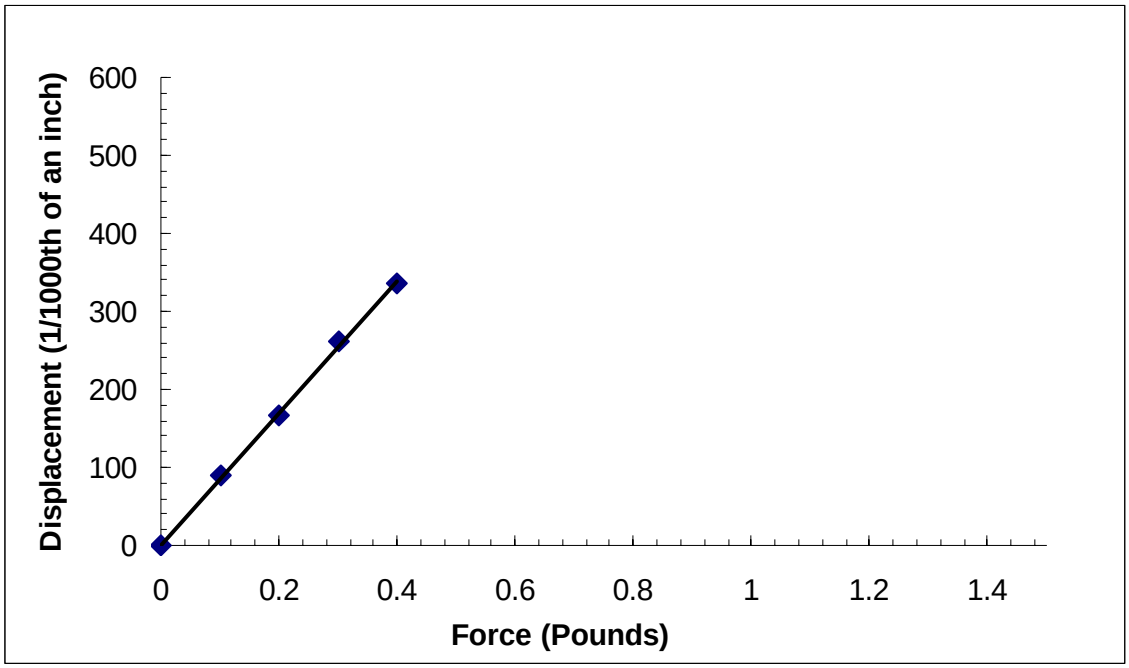

Figure 13: Displacement versus force graph for a cantilever beam of length 7" having a linear fit.

- **Force versus Distance Moved Relations for Bistable Structures**

A model bistable structure was setup as shown in Figure 14. The same hacksaw blades were used again. The snapthrough force and the corresponding snapthrough distance of the beam were tabulated for each beam length under different compressive forces; many such beam lengths were tried. The snapthrough distance versus

snapthrough force for a beam length of 7” at varying compression has been plotted in Figure 15 and given a cubic fit (which was the best fit), i.e., every data point on the curve has been obtained at a different compression.

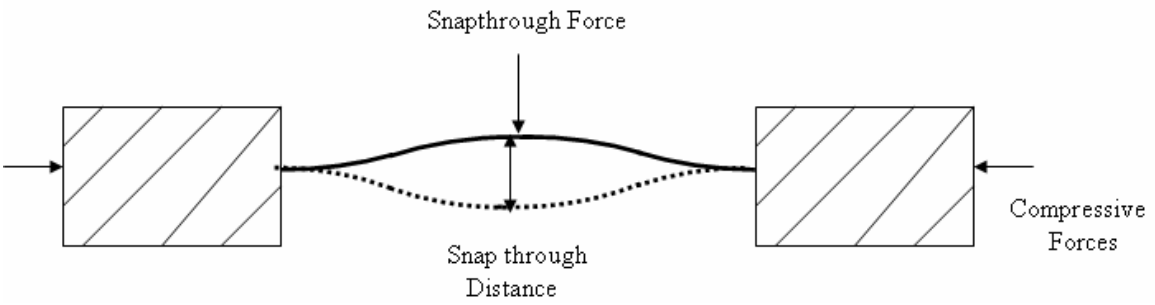

Figure 14: A bistable beam snapping through a certain distance for a snapthrough force at one particular value of compression.

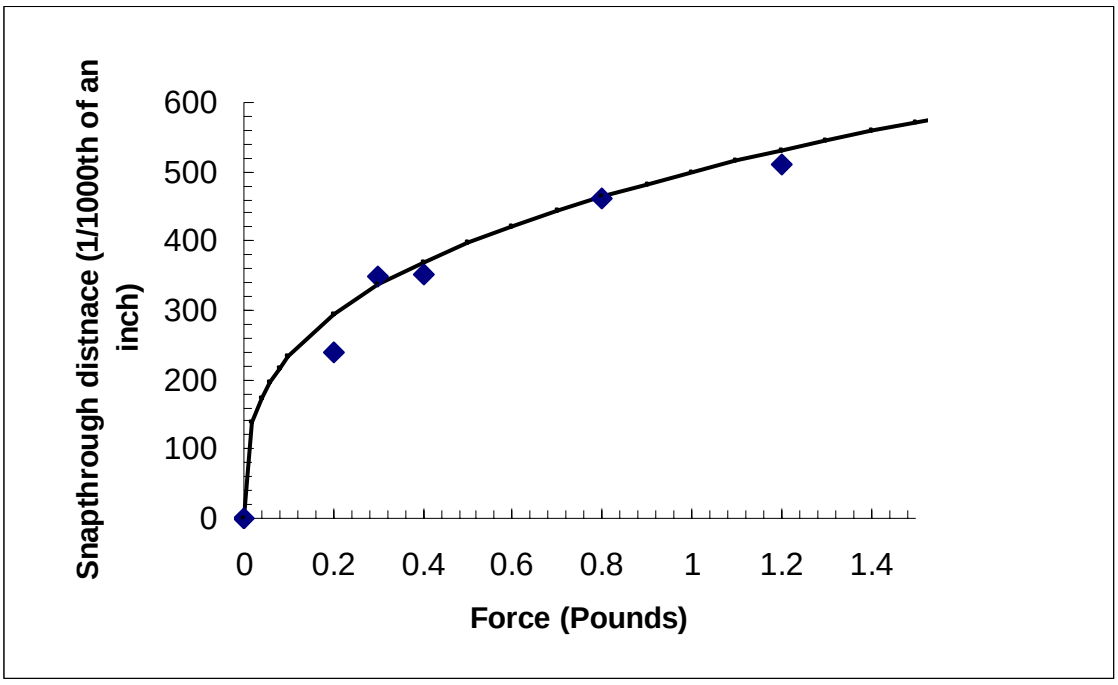

Figure 15: Snapthrough distance versus snap through force for a bistable beam of length 7” at varying compression having a cubic fit.

- **Intersection of Cantilever and Bistable Beams**

  The previous two graphs plotted in Figures 13 and 15 have been plotted together on the same scale in Figure 16. In spite of being dissimilar curves they have a point of intersection. The intersection of the two curves indicates the point where the sensitivity of both the cantilever and the bistable beam of equal length is the same, i.e., given the same force the displacement of the cantilever is the same as the snapthrough distance of the bistable beam (under a certain compression). At values below that point the bistable beam has relatively large displacements compared to cantilever and for points above that it has smaller displacements compared to the cantilever. Hence, if we operate at that point by giving the bistable beam that force which moves it as far as the cantilever, the displacement equations of the cantilever apply to the bistable also.

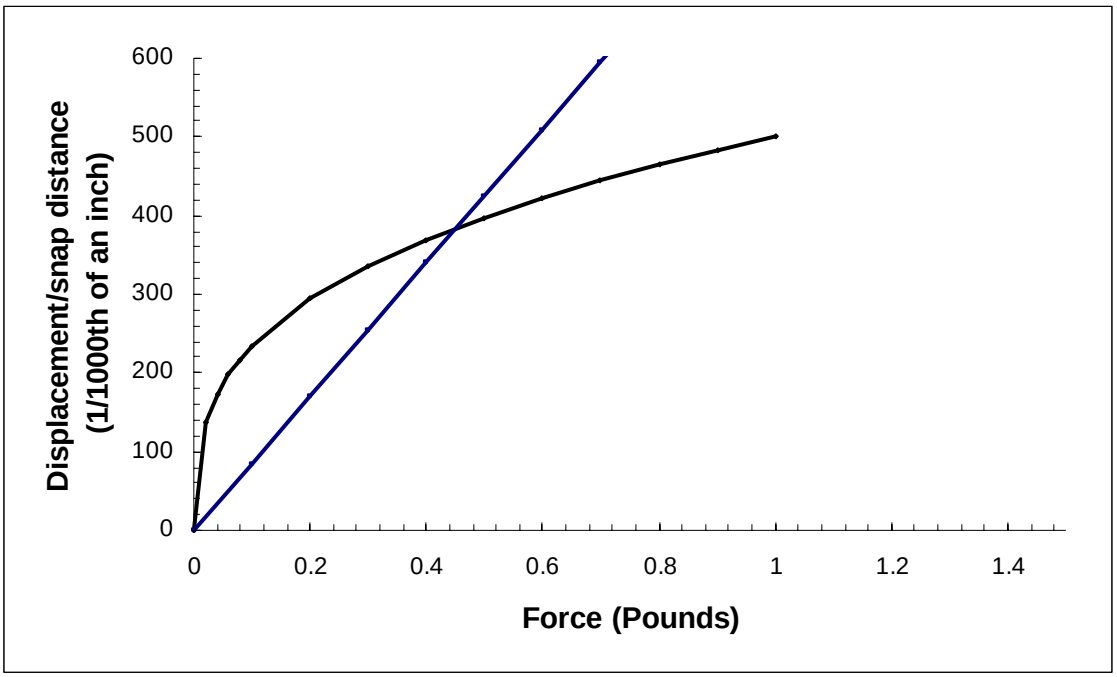

Figure 16: Displacement/snapthrough distance versus force moved by cantilever/bistable beams for the same length of 7" at constant force.

2.3.2 Equation Relating Snapthrough Distance to the Beam Length

Note: D_C is the displacement of a cantilever beam in um and D_B is the snap through distance of a bistable beam in um. D is the displacement when $D_C = D_B$ for beams of same length.

The snapthrough distances of the different bistable beam lengths recorded at a constant force have been considered to get a relation between the length of the beam and the snap distance. The model experiment values obtained for the bistable beams of different lengths have been tabulated in the experimental setup values part of Table 1**.** The hacksaw blades used had a beam of thickness 0.6mm. In order to go down to a thickness of 10um, all parameters were scaled down by a factor of 60 and tabulated in the assumed scaled values part of Table 1. This scaling was done assuming that the steel (the material of the hack saw blade) is comparable in Young's modulus (E) to nickel[1].

The scaled parameters are shown in Figure 17. The curve fit equation was used to find the appropriate constant for the length to snap through distance relation.

The curve was fit to the experimental value highlighted in the table and 6.72 was found to be an appropriate constant. Hence, the first of the design equations was obtained as,

$$D = 6.72l^3 \quad \text{……..……..} \quad (13)$$

where, D is the snap through distance of the bistable beam in um
l is the of the bistable beam in mm

Table 1: Experimental and scaled values of beam length and corresponding snap through distance for a constant force of 0.3 pounds for a bistable beam.

Experimental setup values			**Assumed scaled values (Scaling factor, s = 60)**		
Length (inches) (l)	**Thickness (mm) (t)**	**Snap Distance (D in inches)**	**Length/s (mm)**	**Thickness/s (um)**	**D/s (um)**
5	**0.6**	**0.147**	**2.1**	**10**	**62.2**
6	0.6	0.282	2.54	10	119.3
7	0.6	0.4	2.96	10	169.3
8	0.6	0.617	3.38	10	260

[1] E of nickel is 210 Gpa and that of steel is between 190-210 Gpa

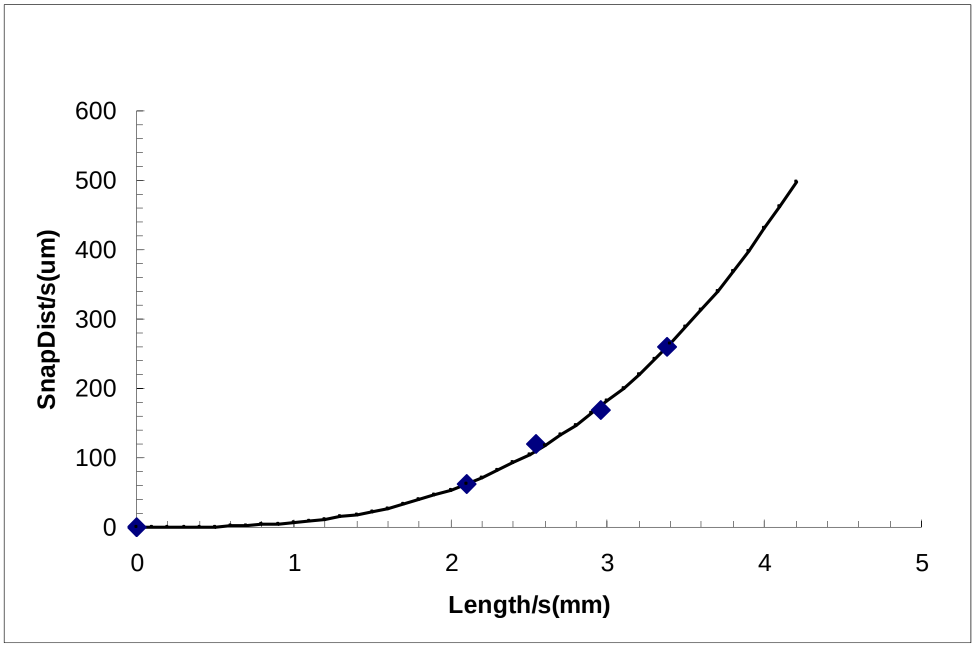

Figure 17: The scaled snapthrough distance versus scaled length of the bistable beam for a constant force.

2.3.3 Equation Relating Voltage Required to Snapthrough Distance

The bistable beam can be operated at a point where given the same force the displacement of a cantilever having the same length as that of the bistable is the same as the snap distance of the bistable beam. That force can be calculated for different bistable beam lengths from the graphs plotted as in Figure 16 for a constant length and the displacement equation of the cantilever beam (Equation 11). This equation of the cantilever applies to the bistable as well at that point of intersection. Hence, Equation 11 can be re-arranged as,

$$V = \sqrt{\frac{Dmgt^3(10^3)}{knl^3}} \quad \ldots\ldots\ldots\ldots\ldots\ldots\ldots\ldots\ldots\ldots\ldots\ldots\ldots.. \quad (14)$$

where, V is the voltage applied (in V)
k is a constant equal to 2.0
n is the number of comb fingers
l is the length of the cantilever beam (in mm)
m is the number of cantilever beams
g is the gap (in um)
t is the thickness of the cantilever beams (in um)
D is the distance moved by the beam (in um)

Taking t=10um, g=10um, m=1 Equation 14 becomes,

$$V = 1000\sqrt{\frac{5000D}{nl^3}}$$

2.3.4 Equation Relating Percent Compression to Snap Through Distance

Consider a thin beam, which bends in a curve which can be approximated as 4 consecutive circular arcs as in Figure 18a. Assume its thickness to be zero, i.e., t=0. Consider the first of the four arcs as shown in Figure 18b; it has been rotated for convenience. It subtends an angle of θ at the center of the circle and has a radius of curvature R. If y is the orthogonal displacement of the first arc, then the displacement for the second arc is 2y, which is also the orthogonal displacement of the bistable beam. When the arc subtends an angle, $\theta = 9.9^0$, the projected length is 0.5% less than the total length of the arcs, and the projected orthogonal displacement (the height of the bump) is 4.3% of the total length. This can be calculated with the simple trigonometry shown in Figure 18b.

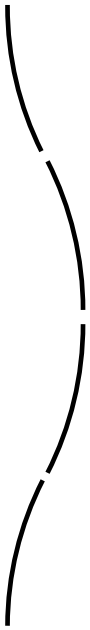

Figure 18a: The bend in a thin beam approximated as four consecutive circular arcs.

For $\theta = 9.9^0$,

Compression in arc = $\dfrac{l' - R \cdot Sin\,9.9^0}{(l' + R \cdot Sin\,9.9^0)/2}$

Length of arc, l' = $R \cdot 9.9^0 \cdot 2\pi / 360$

Hence, we get compression in terms of length = 0.5%

The calculation of orthogonal displacement is,

$y = R \cdot (1 - Cos 9.9^0) = 0.0148R$

The displacement for the bistable beam, 2y = 0.0296R

To get displacement in terms of length:

Total length of arcs,l = 4 × l' = 0.6876R

$\therefore \quad 2y = 0.0433l = 4.3\% \; of \; l$

Similarly, for $\theta = 14.0^0$ the projected height is 1% less than the length and the displacement is 6.1% of the length. More generally, the angle of the arc, and the displacement, are proportional to the square root of the reduction in projected height.

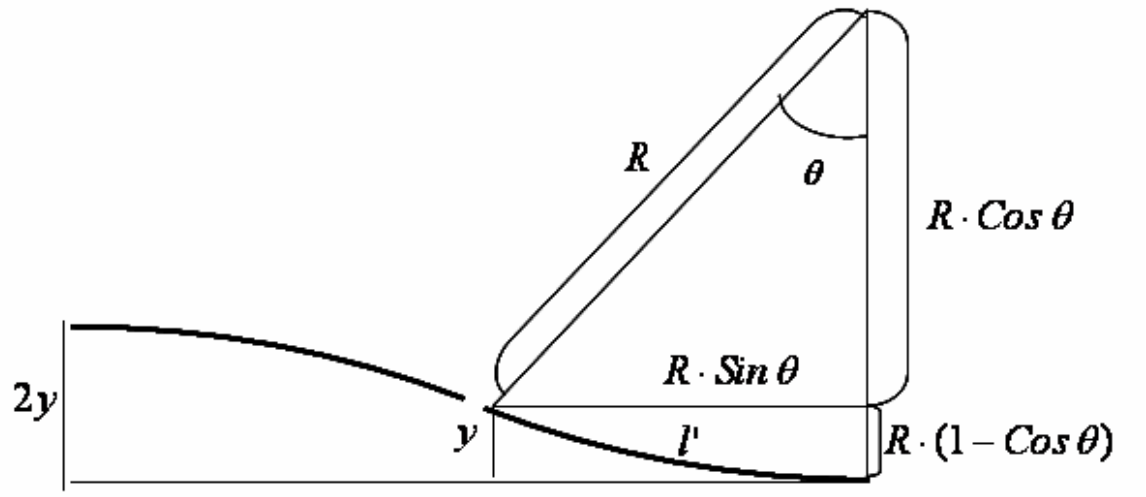

Figure 18b: One of the arcs subtending an angle of θ.

Combining the above derivation of the orthogonal displacement with the fact that this displacement goes as a square root of the compression in percent of the length, we get a relation between the displacement and the compression in terms of the percent length as,

$$C = \left[\frac{D_B}{61l}\right]^2 \quad \text{..... (15)}$$

where, C is the compression in terms of percent of the length

D_B is the snap distance of the bistable beam (2y)

l is the length of the bistable beam

The structures designed are operated at the compression given in equation 15 which is greater than the Euler critical compression for that beam given by equation 10 because the former was derived by approximating the already buckled beam to four circular arcs.

2.3.5 Effect of Scaling in Each of the Above Parameters

If the snapthrough distance is reduced by a factor 'f', then the voltage reduces by a factor of $f^{1.5}$ since the force is proportional to (snap distance)^3 and force is proportional to (voltage)^2 for bistable beams.

The voltage, V_B, needed to obtain a snapthrough distance of D_B, where D_B is given by

$$D_B = \frac{D}{f} \quad \text{..... (16a)}$$

$$V_B = \frac{V}{f^{1.5}} \quad \text{..... (16b)}$$

With some combining

$$V_B = \frac{5800}{\sqrt{nf^3}}$$

The most relevant design equations for t=10um are

$$D = 6.72l^3$$

$$V_B = \frac{5800}{\sqrt{nf^3}} \text{ (For g=10um) or } V_B = 2.592 \times 10^3 \sqrt{\frac{g}{nf^3}} \text{ V}$$

Using Equations 13, 15 and 16 we get

$$C = \frac{0.012\,l^4}{f^2} \quad \text{..... (17)}$$

2.4 Design Based on the Analysis

2.4.1 Dimensions of the Structures Fabricated

A set of dimensions were obtained for various combinations of the length of the beam, the number of combs and the gap between the combs (the thickness of the bistable beam and comb fingers were kept constant at 10um). These were then scaled by a factor 'f' ranging from 1-10. The dimensions that gave the most feasible voltages, snap distances and percent compression in beams were chosen for fabrication. These are tabulated in Table 2.

The structures were designed as shown in Figure 19. The length of the center block (A) supporting the bistable beam structure and the length of the comb fingers were designed based on the snap distance of the beam such that when the beam snaps into either stable state neither do the stationary comb fingers hit the bistable beam nor do the moving comb fingers hit the stationary comb. Therefore the lengths of the comb fingers were double the snap distance in one direction. The anchors were designed to be massive and are typically 500um × 500um.

The values tabulated in Table 2 are those which were finally chosen and used for fabrication. The 20 different structures were placed in 4 rows and 5 columns on a 3" × 2" glass substrate. They were picked by varying L, n, g, and f and then choosing the sets with the most reasonable voltages, compression values and snap distances. The structures 1 and 4 are cantilever structures whose anchors on one side are 30um × 100um.

For example, if structure 6 from the set of values in Table 2 is considered, for the given set of its dimensions it would snap through a distance of 102um when given a voltage of 63V and for the compression in nickel to be 0.13% of the length.

Note: Figure not to scale

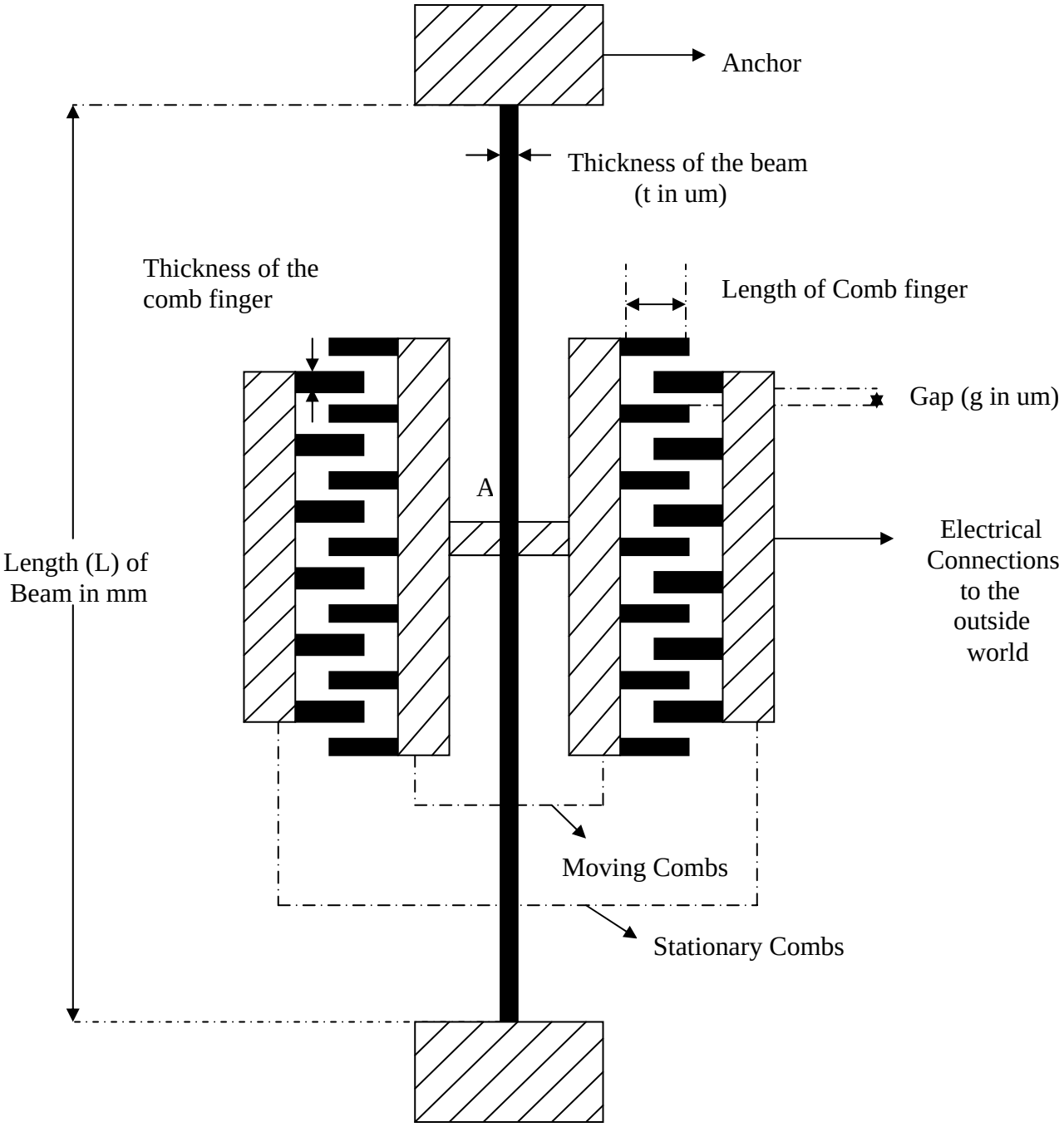

Figure 19: Figure showing the bistable beam structure and its parts as designed.

Table 2: Dimensions of the 20 structures chosen for fabrication.

Fig No.	Length of beam(mm)	Number of comb fingers (n)	Gap between the combs (g)(um)	Length of comb finger (um)	Scaling factor (f)	Snap distance (D_B in um)	Voltage (V_B in V)	%comp in terms of length
1	3.5	50	10	136.04	3	96.04	157.7621	0.202352
2	4.5	60	10	127.48	7	87.48	40.4061	0.101562
3	4.5	40	10	142.06	6	102.06	62.36096	0.138238
4	3.7	10	20	125.097	4	85.09704	324.037	0.142156
5	4.6	40	40	133.4426	7	93.44256	98.97433	0.110896
6	4	50	20	183.36	3	143.36	223.1093	0.345204
7	4.8	40	30	146.1683	7	106.1683	85.71429	0.131476
8	4.6	40	40	226.8851	7	186.8851	98.97433	0.110896
9	4.3	25	20	146.8574	5	106.8574	146.6424	0.165964
10	4.6	50	20	170.8196	5	130.8196	103.6919	0.217355
11	4.2	20	45	122.9786	6	82.97856	187.0829	0.1049
12	3.7	30	20	108.0776	5	68.07763	133.8656	0.09098
13	3.4	50	10	106.0307	4	66.03072	102.4695	0.101362
14	4.3	30	30	116.3267	7	76.32672	98.97433	0.084675
15	3.9	70	10	119.7247	5	79.72474	61.96773	0.112305
16	3	50	10	100.48	3	60.48	157.7621	0.109225
17	3.5	30	15	97.624	5	57.624	115.931	0.072847
18	3.7	50	25	96.73136	6	56.73136	88.19171	0.063181
19	3.5	30	35	97.624	5	57.624	177.0875	0.072847
20	3.6	70	5	102.7057	5	62.70566	43.8178	0.081536

3. Experimental Setup

3.1 Mask Making

3.1.1 Mask Layout and Generation

The patterning of the structures was done using two levels. The first level mask was designed for patterning the sacrificial layer (AZ P4620) which was10um thick. The purpose of this layer is to release the bistable beam and the comb fingers from the surface later on in the processing by dissolving the sacrificial layer [2]. The second level mask was designed for patterning the actual structures in negative SU-8 50 resist. This resist was used because it serves as a good electroplating mould for high aspect ratio MEMS structures [2]. The Mann 3600 pattern generator at CAMD (Fig 20) was used to pattern the masks. It is designed for patterning standard 5" × 5" mask plates for use in optical lithography. Pattern designs are created in AutoCAD. The AutoCAD file is then converted into binary format, which can be fractured into data read by the pattern generator. The masks designed are shown in Chapter 4.

Figure 20: The Mann 3600 pattern generator at CAMD [8].

3.1.2 Two Level Alignment

In order to align the two levels when exposing the second level, alignment marks were used as shown. The lighter parts are opaque on the masks in all these figures. Figure 21a shows the alignment mark patterned on the first level. The size of the square is 250 × 250 um and the cross has a total height of 140 um and the width of its arms is 50um.

The marks shown in Figure 21b are the alignment marks used on the second level. The size of the outer square is 350 × 350 um and that of the inner square is 300 × 300 um. The broken cross marks are 50 um in width. The alignment of the two levels happens when the alignment marks appear as shown in Figure 21c. All the figures of alignment marks in 21 were taken directly from the mask's 1 and 2, and the alignment marks on figure 21c was taken by aligning both the masks. A set of two alignment marks was sufficient for proper alignment of the two levels but there were three alignment marks placed on each substrate. This is done for safety in case one should be damaged during processing. An alignment error of 20um can be compensated for on the substrate.

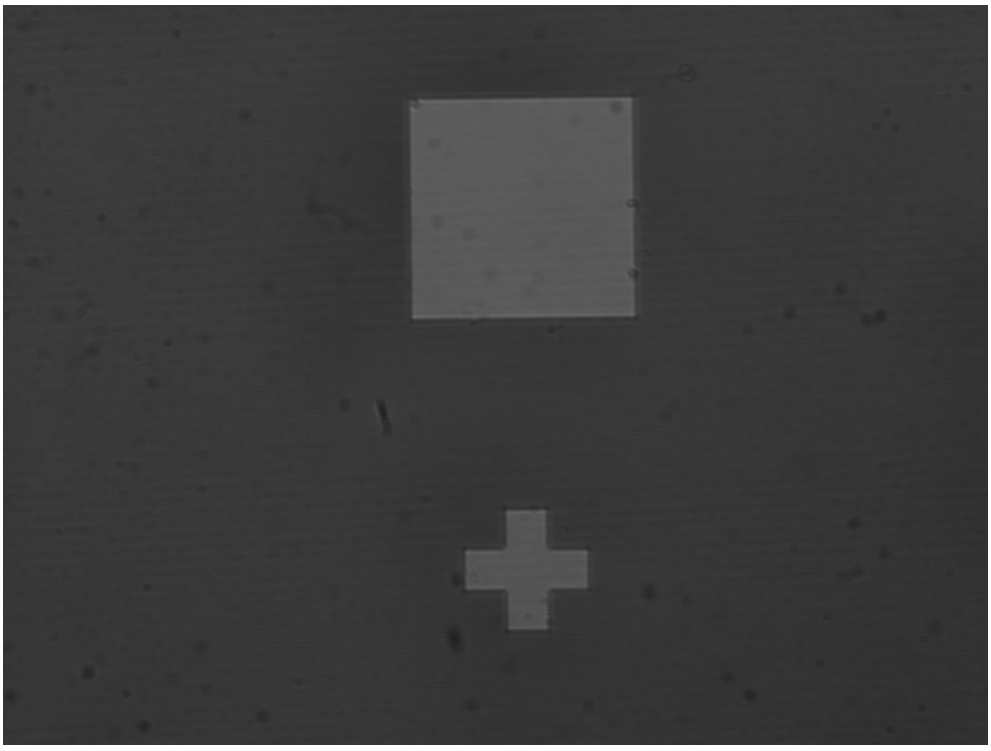

Figure21a: Alignment marks on the first level.

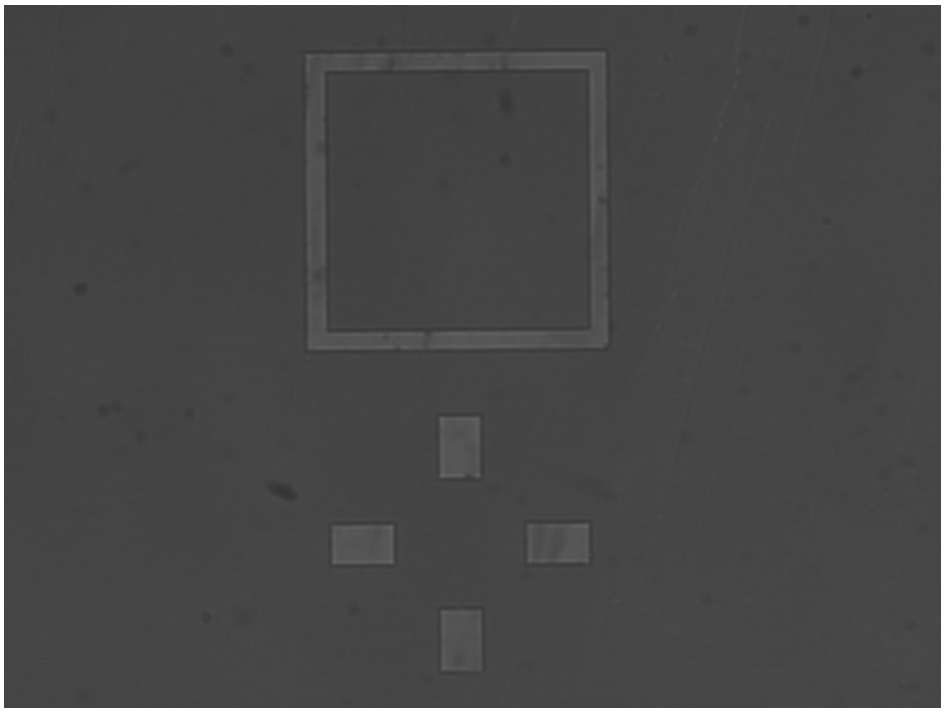

Figure 21b: Alignment marks on the second level.

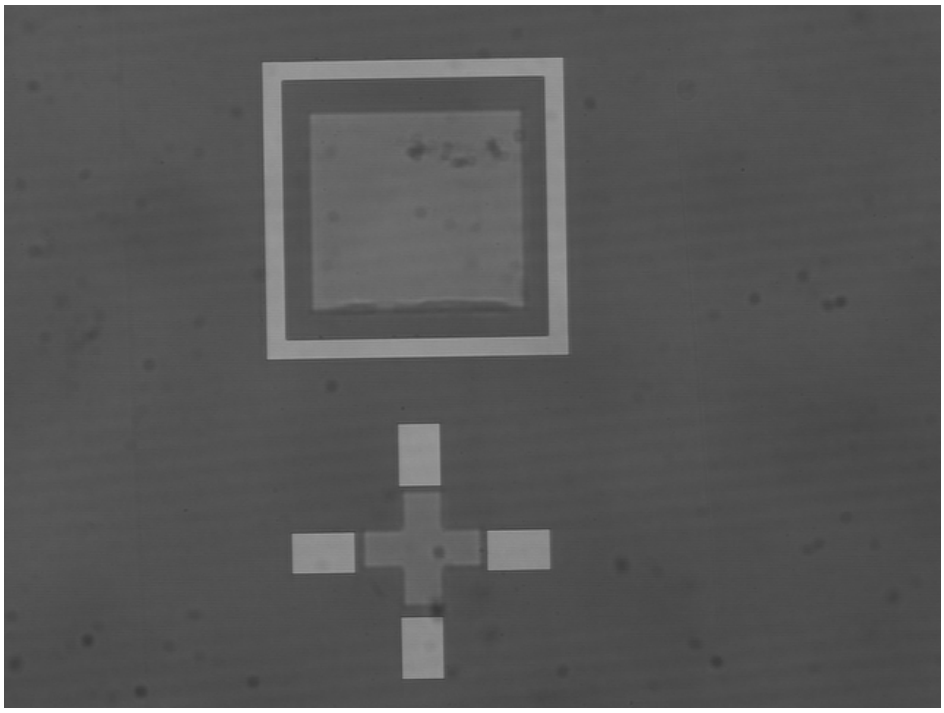

Figure 21c: Marks on both levels obtained by aligning the masks. The alignment marks on the first level appear thinner than their actual dimensions since they are out of focus.

3.2 Sample Making

3.2.1 Patterning First Level of Positive AZP4620 Resist

- **Spin Coating and Soft Baking**

The positive resist had to be 10um thick. Therefore AZ P4620 positive resist was used. This is a product of the Clariant Company. The spin cycle used to get a thickness of 10um is shown in Figure 22. The ramp rate of the first step was 100rpm/sec and the ramp rates of the remaining steps are 200rpm/sec. The sample was then soft baked at 110^0C for 200seconds in a conventional oven.

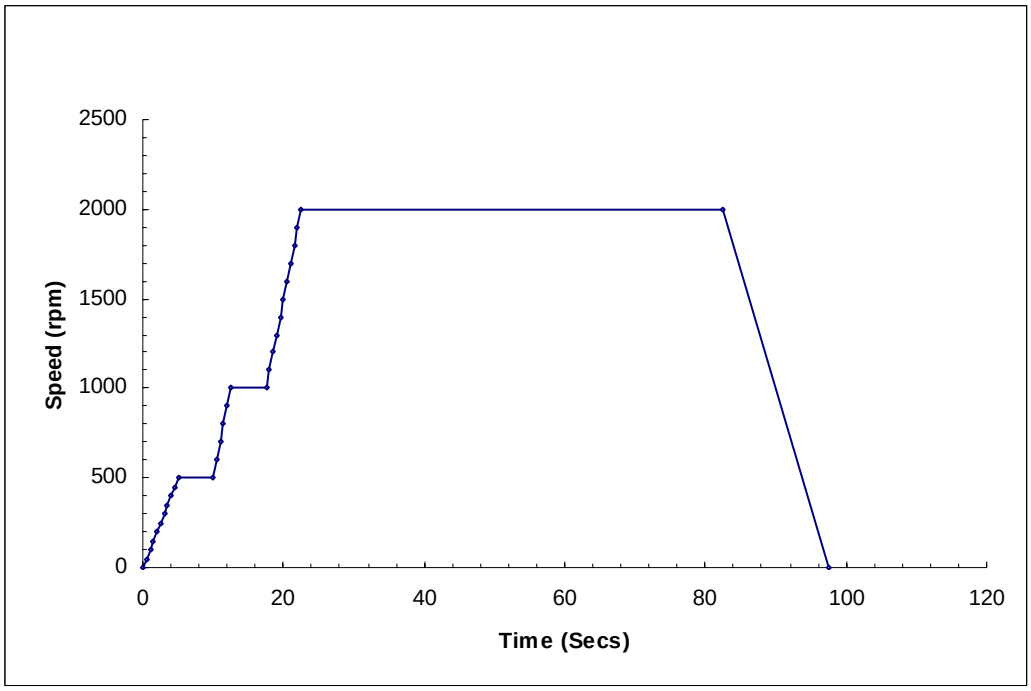

Figure 22: Spin cycle for 10um of AZ P4620 resist.

- **UV Exposure**

The next stage in the processing was UV exposure. The Quintel Q4000 aligner is used in the EMDL. Contact printing was done with an exposure dose of 240mJ/cm^2. The intensity of the light varied from 2-4mW/cm^2 and was always measured at the time of exposure. The exposure time for a dose of 240mJ/cm^2 and intensity of 4mW/cm^2 is, $\frac{240mJ/cm^2}{4mW/cm^2}$=65 secs.

Figure 23: The Quintel Q4000 aligner at EMDL [7].

- **PEB (Post Exposure Bake) and Development**

Post exposure baking helps evaporate the solvent, but for a thickness as low as 10um it is an optional step and was skipped in this case. Hence, the sample was directly taken for developing after exposure. The developer was AZ 400K Developer used in a 1:3 ratio with DI water. The development process took about 1.5minutes. The time for development varies depending on the resist thickness. The sample was then rinsed with DI water.

- **Hard Baking**

There has always been a problem with two level resists in which the bottom layer is affected by the processing steps of the next level (in this case negative SU 8-50 resist). Such problems were discussed and solved [2]. It was suggested that a thicker adhesion layer and plating base (discussed in the section below) would improve the situation. The downside of this for thick resists such as AZ P4620 is the layer would have to be very thick. Instead the hard baking time was increased to 200^{0}C for 3hrs for AZ P4620. This was the method adopted for hard baking the sample.

3.2.2 Sputtering of Ti and Cu

In order to electroplate at a later stage, copper was used as a plating base. Unfortunately, copper has very poor adhesion to glass and so titanium was used as an adhesion layer between copper and the glass substrate. The deposition of the layers is

done through DC and RF sputtering respectively for Ti and Cu. The Edwards Coating System–E306A (shown in Figure 24) in EMDL was used for sputtering 100nm of Ti and 200nm of Cu. The pre-deposition sputtering pressure used was 1×10^{-5} Torr, RF power was 200 W and the working pressure was 1×10^{-2} Torr (at room temperature). The deposition rates for Ti and Cu were 12.76um/min and 16um/min respectively at these parameters. The reflected power in the system must always be at minimum since it results from a mismatch between the power supply impedance and the reaction chamber impedance.

Figure 24: The Edwards Coating System–E306A at EMDL [7].

3.2.3 Patterning Second Level of Negative SU-8 50 Resist

- **Spin Coating and Soft Baking**

SU8 -50 resist from Microchem was used for patterning the second level. This is a negative tone resist. 2 ml of the resist was dispensed onto the sample placed on the spinner chuck. The spin cycles used for thicknesses of 100um and 40um are shown in

figures 25a and 25b respectively. The sample was baked immediately after spin coating in a conventional oven. The temperature of the oven was ramped up to 96^0C at the rate of 5^0C/min starting from the room temperature of 25-30^{0}C and then held at 96^0C for 85 minutes (for the 100um thickness) and for 45minutes (for the 40um thickness). The sample was then cooled for a couple of hours before proceeding; this was done to avoid any stress related problems which are common in SU 8 resists.

- **Exposing and Post Exposure Baking (PEB)**

The sample was exposed using the Quintel Q4000 Aligner. The mask was in contact with the substrate. The exposure dose required for each thickness was:
T=100um: 400mJ/cm^2
T=40um: 190mJ/ cm^2
The UV dosage increases with the resist thickness because a thicker layer of the resist has more area exposed for cross linking to happen, and so requires a longer time for exposure. The sample was then baked after exposure as this aids in the exposure induced photo reaction. The temperature of the oven was ramped to 96^0C at the rate of 5^0C/min from 25^0C. Then the oven was held at 96^0C for 15min (for 100um thickness) and for 9min (for 40um thickness). The substrate was then left to cool for a couple of hours.

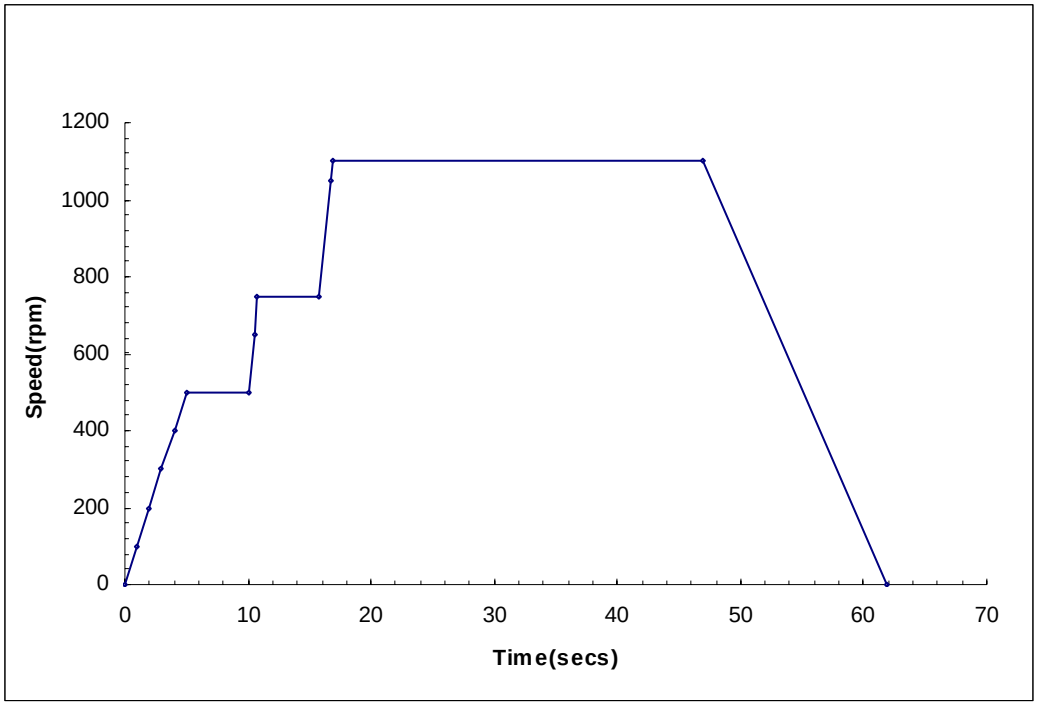

Fig 25a: Spin cycle of 100um thick SU 8-50 resist.

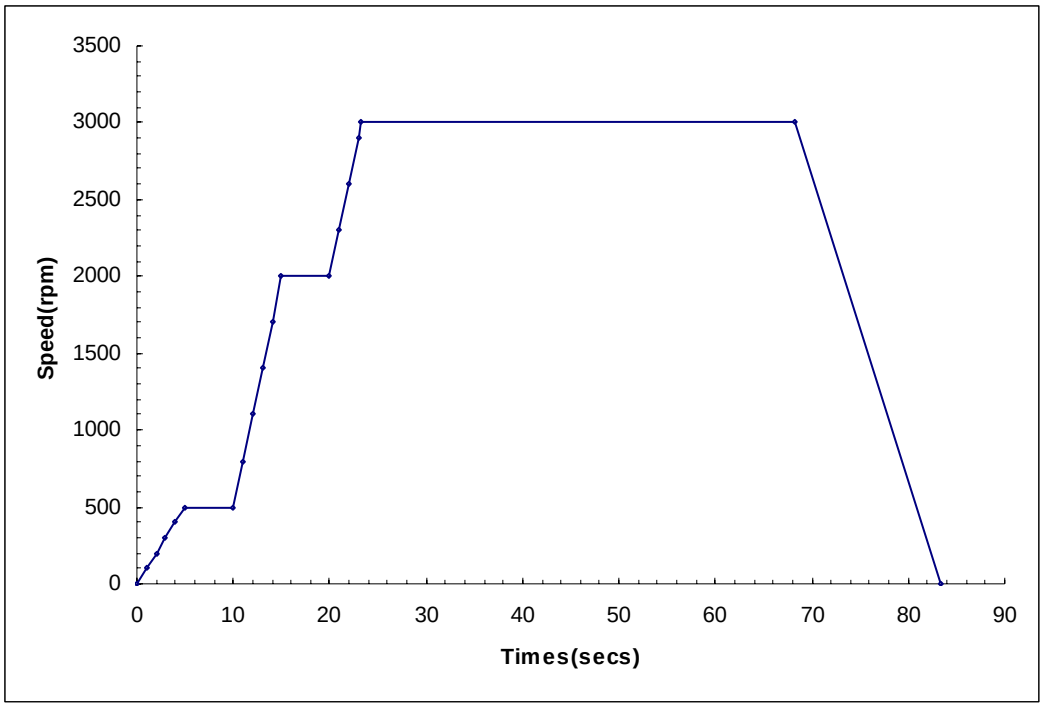

Fig 25b: Spin cycle of 40um thick SU 8-50 resist.

- **Developing and Hard Baking**

The developer used for SU 8-50 is SU-8 developer by Microchem which was used undiluted. Different kinds of developing techniques were used:

1. Mechanical stirring at different temperatures and rpm's.
   (a) Mechanical stirring with a stand at room temperature at 150 rpm.

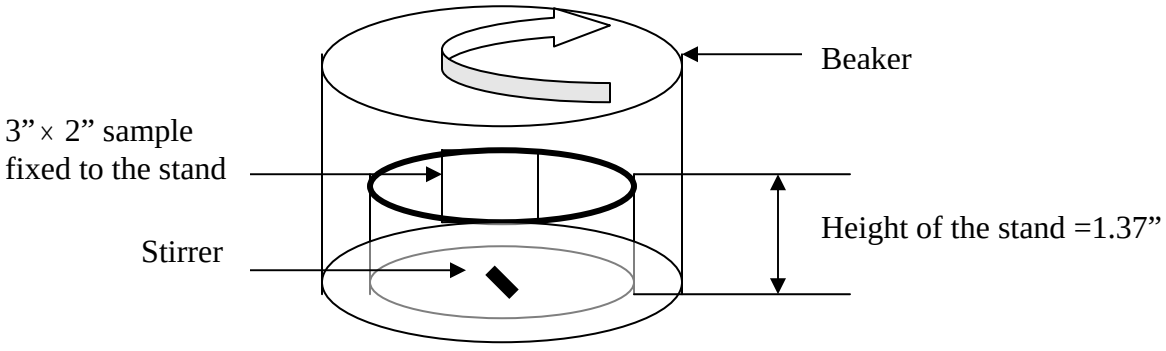

Fig 26a: Mechanical stirring with the sample fixed on a stand above the stirrer.

(b) Mechanical stirring at room temperature in a Petri dish with rotation of sample at 250 rpm (for reasons discussed in Chapter 4).

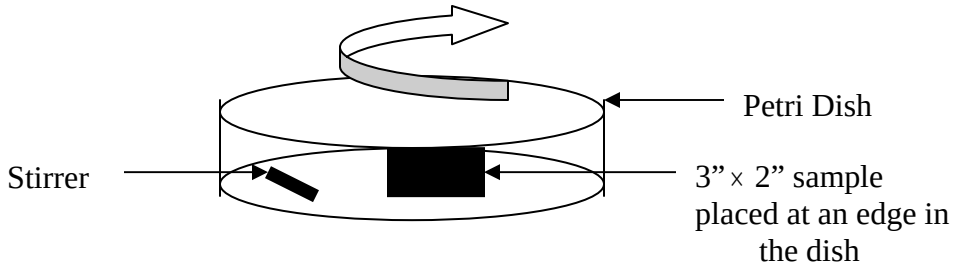

Fig 26b: Mechanical stirring with the sample offset in a petri dish beside the stirrer.

(c) Mechanical stirring at 50^0C.

2. Ultrasonic development at room temperature.

After developing the structures, hard baking is necessary to improve the resist adhesion to the sample for electroplating, else it peels away. The samples were baked at 130^0C for 30 minutes. The drawback of this was that it increased the time taken for resist removal after electroplating.

3.2.4 Nickel Electroplating

- **Basics in Electrodeposition**

Nickel electroplating is similar to other electro deposition processes that employ soluble metal anodes; that is, direct current is made to flow between two electrodes immersed in a conductive, aqueous solution of nickel salts. The flow of direct current causes one of the electrodes (the anode) to dissolve and the other electrode (the cathode) to be come covered with nickel (as shown in Figure 27).

Calculation of Average Coating Thickness [4]

The amount of nickel deposited at the cathode and the amount dissolved at the anode are directly proportional to the product of the current and the time and may be calculated from the following expression:

$$m = \frac{M}{nF}(a)(I)(t) \quad \text{.....} \quad \text{(18a)}$$

where, m is the amount of nickel deposited at the cathode (or dissolved at the anode) in grams
I is the current that flows through the plating tank in amperes
t is the time that the current flows in Hours
a is the current efficiency normally taken as 0.955 for cathode (for calculations)
M is the atomic weight of nickel (in grams)
n is the number of electrons in the electrochemical reaction

F is the Faraday's constant (in ampere-hours)

$$\frac{M}{nF} = \frac{58.69}{(2)(26.799)} = 1.095\frac{grams}{ampere.hour}$$

this was the proportionality constant.

Hence

$$m = 1.095\,(a)\,(I)\,(t) \quad \ldots\ldots\ldots\ldots\ldots\ldots\ldots\ldots \text{(18b)}$$

The nickel thickness in um, can be derived from 18b by dividing it by the density of nickel (d=8.907g cm^{-3}), and the surface area to be electroplated (A in cm^2) as,

$$s = \frac{(m)}{(d)\,(A)} = \frac{(1.095)\,(a)\,(I)\,(t)}{(8.097)\,(A)} = \frac{0.12294\,(a)\,(I)\,(t)(10^4)}{(A)} \quad \ldots\ldots\ldots\ldots \text{(19)}$$

The ratio, I/A is the current density (in A/cm^2). Hence, the amount of nickel deposited depends on the current density and the time as seen from 19.

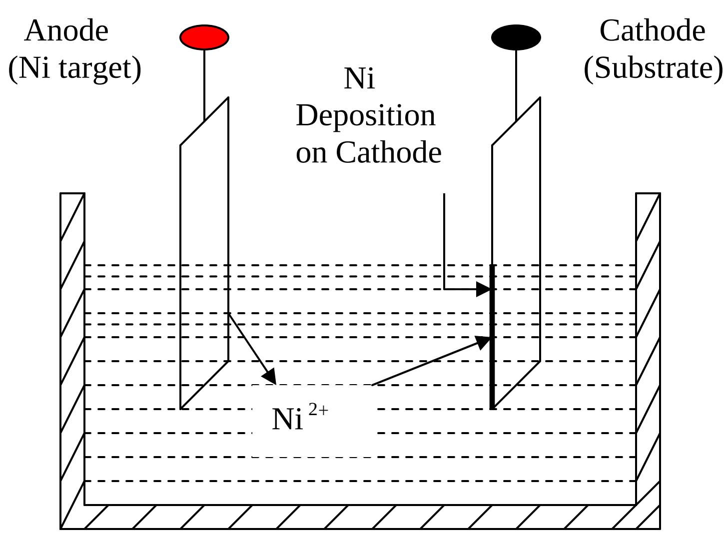

Figure 27: Schematic of an electroplating setup.

- **Dimensions of Electroplating Setup and Plating Solution Used**

The electroplating setup was constructed using a polypropylene tank with a lid having dimensions as shown in Figure 28. This plating tank goes into a constant temperature water bath. The holders for the nickel target and the sample were made to

hold 3" × 2" rectangular glass wafers and were placed 6" apart. All the screws used were stainless steel to minimize corrosion inside the setup. The stirrer used was made of polypropylene and was placed exactly mid way between the holders. The spacing between the electrodes, the stirrer, etc., is shown in the Figure 28.

The speed of rotation is controlled by the voltage given to the AC motor. The right speed of rotation for the stirrer has to be found at which it would uniformly plate the sample. The speed of 240rpm was found appropriate. The setup is shown in Figure 29. This setup has the advantages of being relatively compact and inexpensive.

The nickel plating solution used is Nickel Sulfamate which is used for high aspect ratio plating. The bath operates at a pH = 4.0 and a bath temperature between 52-55 ^{0}C, under continuous stirring. The stirring is required to maintain uniformity in the solution while plating. The plating solution composition is shown in Table 3. Lauryl Sulfate is used to remove hydrogen gas and reduce surface tension. To maintain the pH from time to time Sodium Hydroxide (NaOH) or Sulfuric Acid (H_2SO_4) is added. The use of the acid H_2SO_4 will increase the hydrogen ion concentration (H^+) and will reduce the pH of the solution. NaOH does the reverse and increases the pH.

3.2.5 Resist Stripping

The SU 8 removal is done using a standard solution called Nano Remover PG which is a NMP based solvent stripper designed for efficient and complete removal of SU-8, and is manufactured from Microchem. Stripping is done in immersion mode with a two bath system both containing the remover PG, at temperatures between 77-78 ^{0}C. The first bath removes the bulk of the resist, and the second cleaner bath removes the traces of material. A third bath of a water miscible solvent like IPA is used at room temperature to serve as a final solvent rinse prior to DI water rinse and dry. The process performed used no mechanical or ultrasonic agitation. The time of removal was about 35-40min in fresh solution baths. The long time periods are a consequence of the hard baking done for the resist.

Table 3: Composition of Nickel Sulfamate Solution used for plating.

Chemical	*Amount*
$Ni(SO_3NH_2)_2$ (Nickel Sulfamate)	450 mL
H_3BO_3 (Boric Acid)	37.5g
Lauryl Sulfate	3g
Add DI water to make it up to 1000mL	

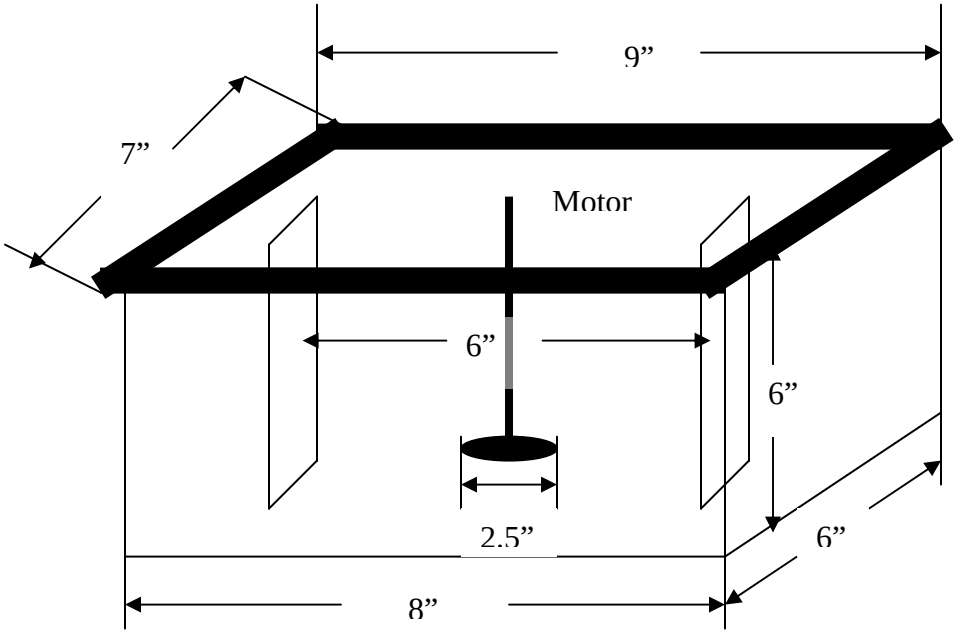

Figure 28: Diagram showing the dimensions of the electroplating setup.

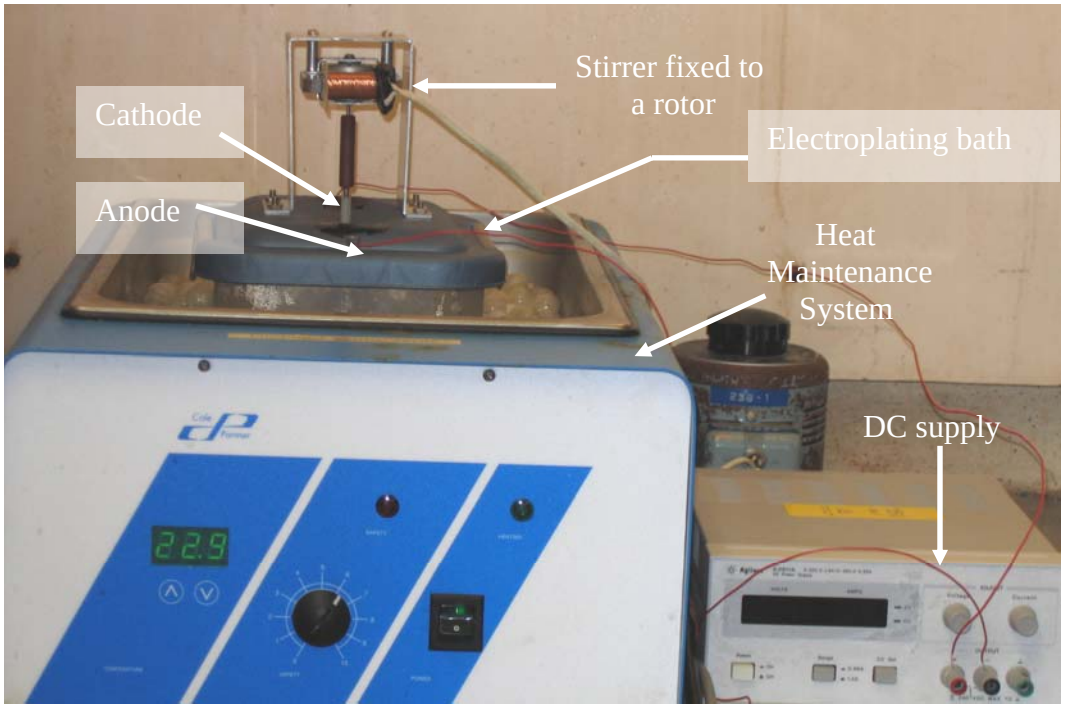

Figure 29: The electroplating setup used.

4. Results and Discussions

4.1: Masks Made

Figure 30 shows the AutoCAD file of mask 1 which was used for patterning the sacrificial layers for all the 20 structures. The rectangular sections provide a sacrificial layer under the entire bistable beam, the moving combs and the stationary combs with an additional 20um given in each dimension as an error margin. The alignment marks discussed in section 3.2.2 are too small to be seen in Figure 30 and 31. They were placed between the second and third row of the structures.

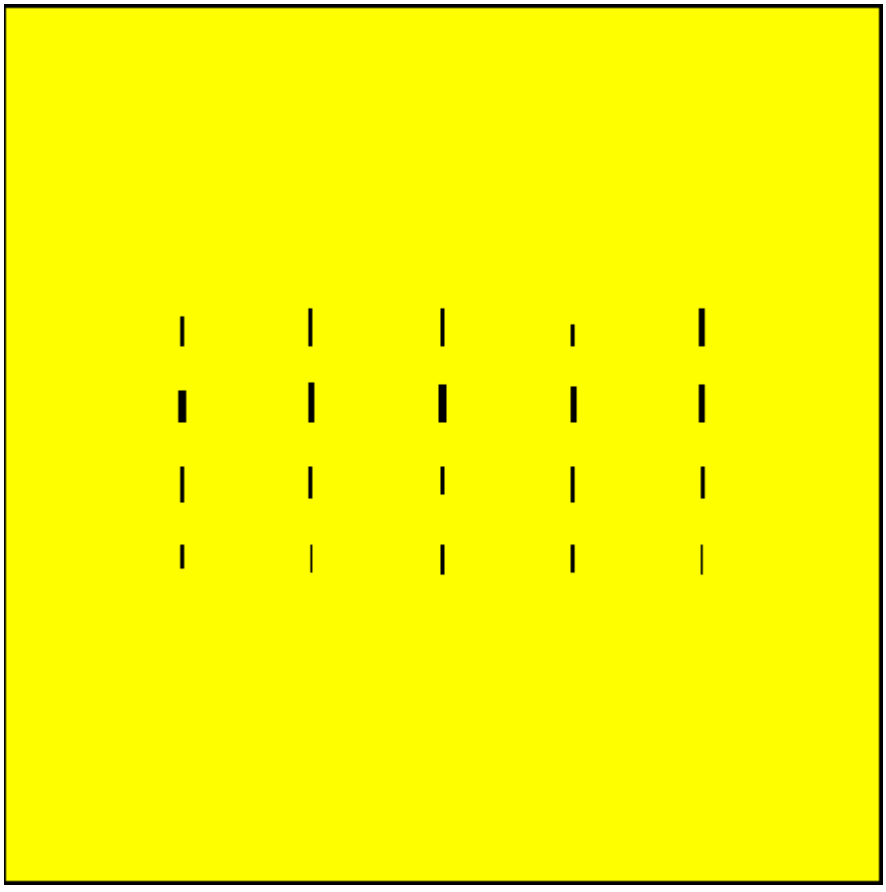

Figure 30: Mask 1, for patterning the sacrificial layer with AZ P4620 (positive tone resist).

Figure 31a shows the AutoCAD file of mask 2 which patterns the structures in a negative tone resist. Figure 31b shows an enlarged picture of one particular structure from mask 2. The alignments marks are too small to be seen in the figures.

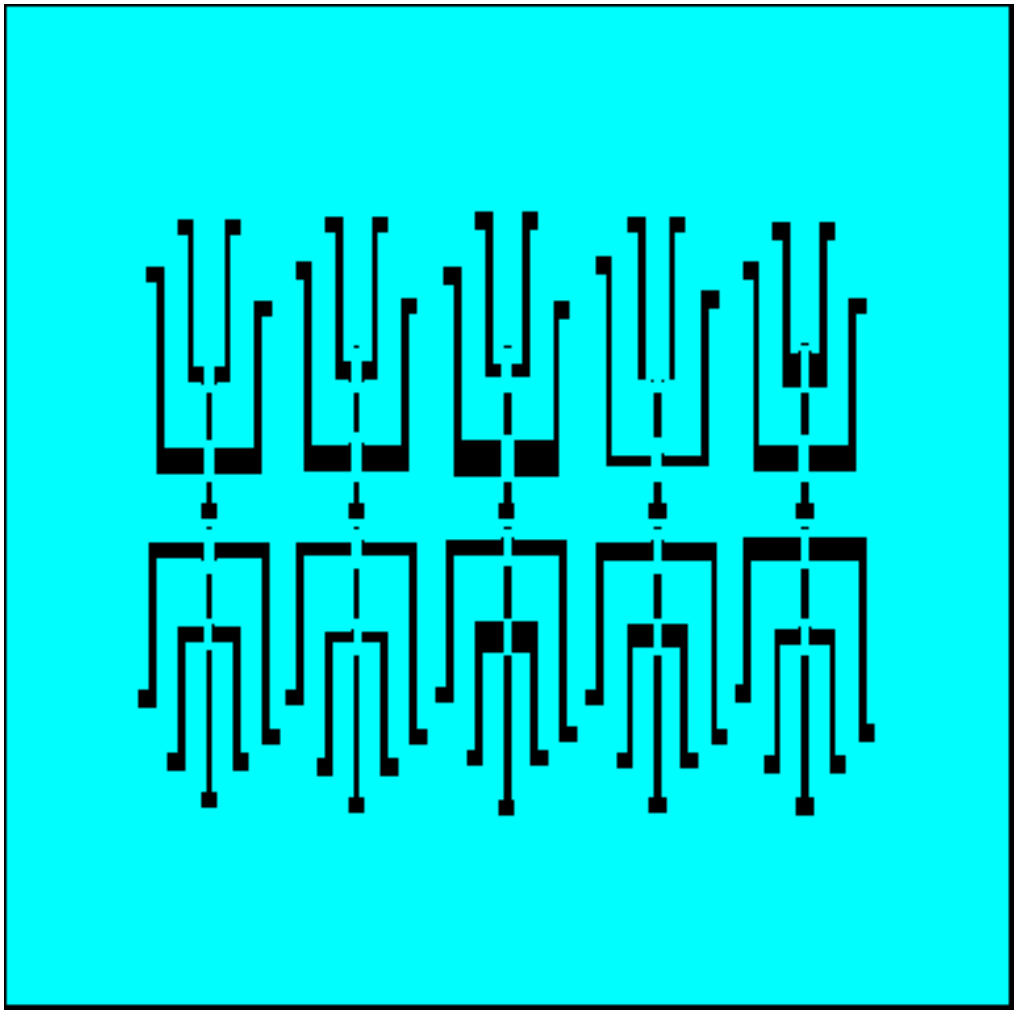

Figure 31a: Mask 2, for patterning the electroplating mould with SU 8-50 (negative tone resist).

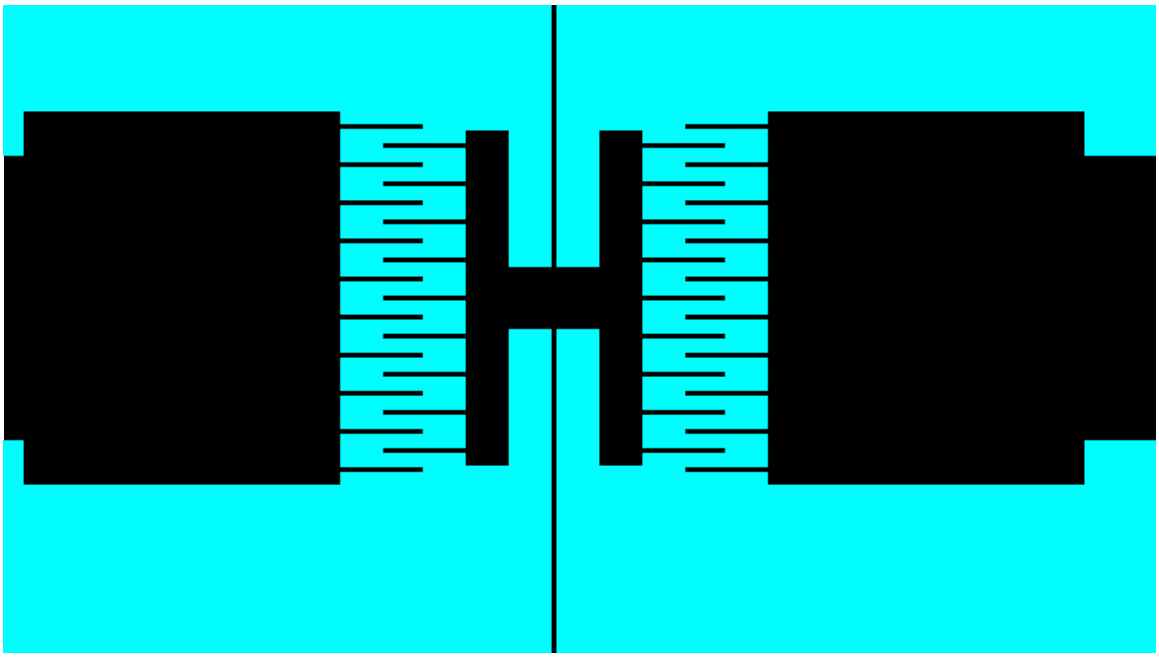

Figure 31b: Enlarged image of structure 4 from mask2 (anchors are not seen in the picture).

4.2 Characteristics of Electroplating Setup

The observed plating rate for different plating current densities is shown in Figure 32.

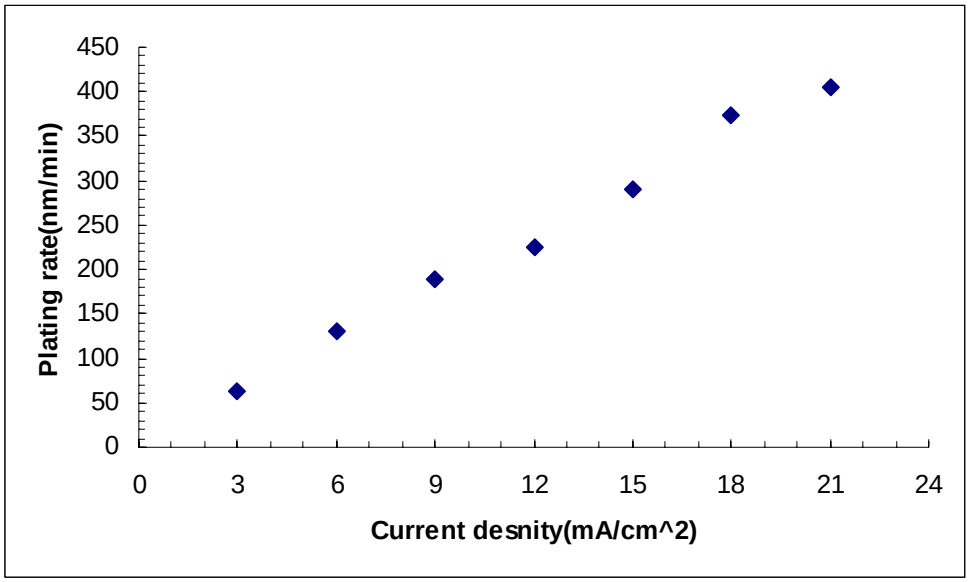

Figure 32: Plating rate versus plating current density for the nickel sulfamate solution at a pH=4.0 and a temperature of 53^{0}C.

The average surface roughness (Ra) varies with the current density. The Ra of the surface at different plating current densities is shown in Figure 33. The average roughness was measured using the AFM at EMDL. The measurement of this roughness is given by,

$$R_a = \frac{\sum_{t}^{N} \left| Z_i - \bar{Z} \right|}{N}$$

Where, $\bar{Z} = \frac{\sum_{t}^{N} Z_i}{N}$

and, N is the total number of points.

Figure 33 shows that the average roughness of the surface increases initially with the current density and then remains mostly constant at the higher current densities. At higher current densities the roughness is comparable to $\frac{\lambda}{4}$ for visible light. This implies the moving beam would be unsuitable for operation in reflection as too much light would be scattered.

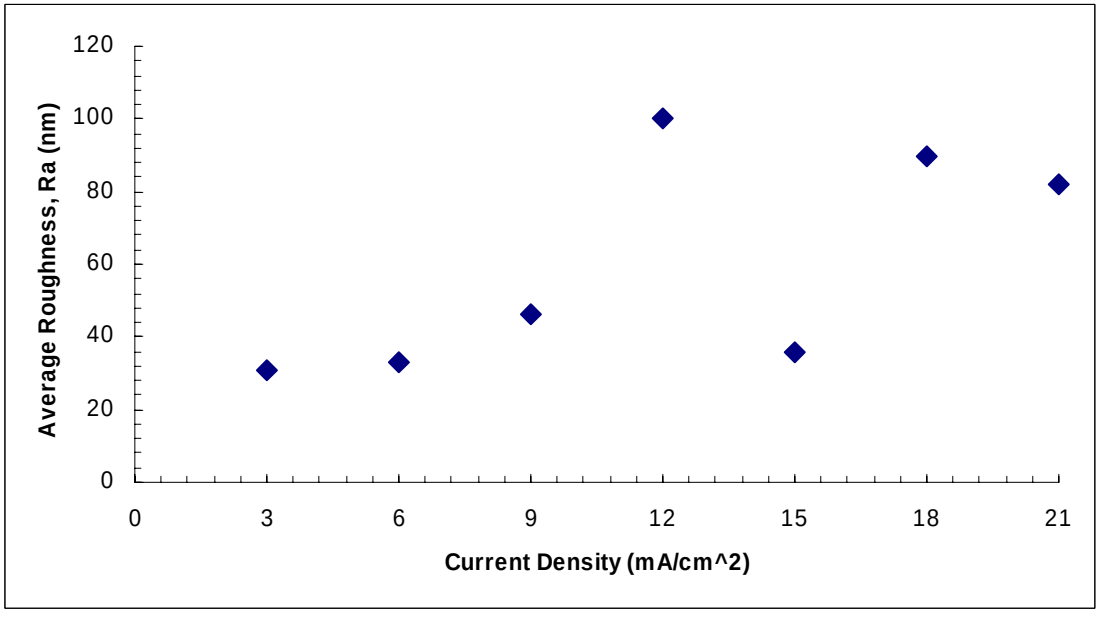

Figure 33: Roughness of the surface versus plating current density for the nickel sulfamate solution at a pH=4.0 and a temperature of 53^0C.

The current density used for plating the structures was $3.3 mA/cm^2$. The d-space at different current densities needs to be calculated by the X-ray diffraction method for this particular composition of nickel plating solution at a pH=4.0. That would help

determine the compression in the beam at different current densities. Then the beam can be plated with the current density that gives the compression closest to desired (Compression tabulated in Table 2).

4.3 Effect of Different Developing Techniques

Note: The substrate was placed upside down [10] in all the developing techniques used. This helped the resist to get removed more easily during developing.
This section discusses the effect of various developing techniques used such mechanical stirring (with and without heating) and ultrasonic development on 100um thick SU8-50. It also discusses the improvements found with similar processes for reduced aspect ratio of the structures (for a resist thickness of 40um).

- **For 100um Thick SU8-50 Resist**

Mechanical stirring at a temperature of 50^0C made the developer too active. This caused the SU8 -50 resist to peel from the surface before the entire thickness of the resist developed. Stirring at speeds above 150rpm also caused the resist to peel from the surface.

Mechanical stirring at room temperature

The substrate was then developed at room temperature. This allowed the substrate to be in contact with the developer for a longer time without peeling and also gave the developer more time to reach down through the entire thickness of the resist than before. The stirring was done at 150rpm since the higher speeds failed. The pictures shown in Figure 34 are of structure 15 (from table2) developed at 150rpm, at room temperature (as in Figure 26a). They were photographed on edge using an Olympus BX60 microscope in bright field. They show complete development of the comb fingers through the entire thickness of the resist. The comb finger thickness in the figure is 10um and the gap between the combs seen is 30um. The lighter areas seen in Figure 34 are the resist regions. The thickness of the comb finger developed is larger at the bottom of the resist (i.e., the substrate end seen on the left portion of the pictures) than it is towards the top. This is due to more exposure of the resist at the top compared to the bottom.

Following this examination, more samples were made in the same manner as above. These samples were then plated 30um tall at a current density of $3.3mA/cm^2$ and then the SU8-50 was stripped. The photographed samples of structure 16 (Table 2) are shown in Figures 35 and 36. The bubbles seen in the photograph were caused by evolution of hydrogen during DC plating.

Summarizing all the structures on the substrate, bistable beam lengths of up to 250um were developed and plated along the entire length of the beam. Comb fingers of all sizes and gaps were developed.

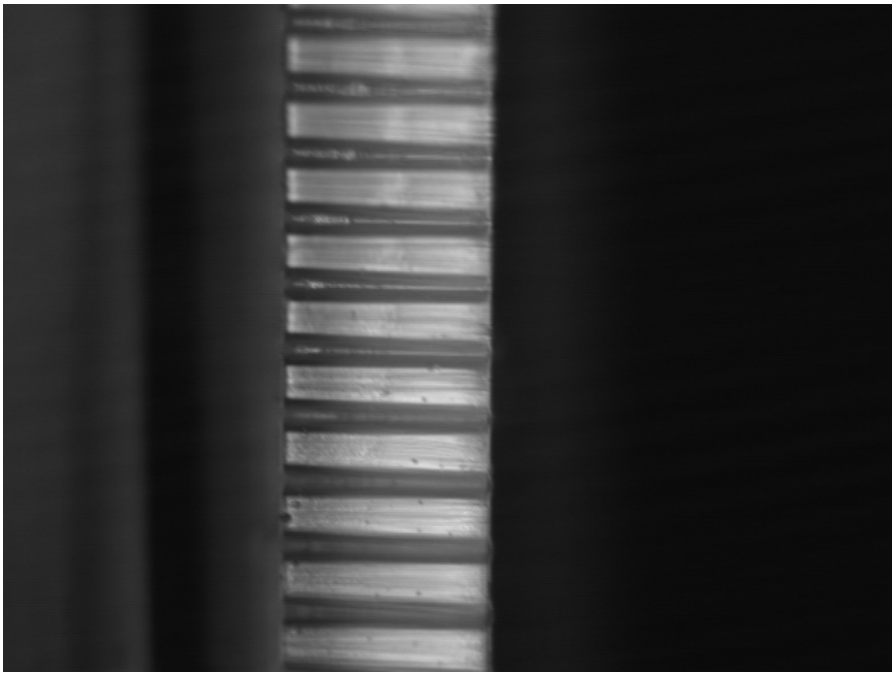

(a)

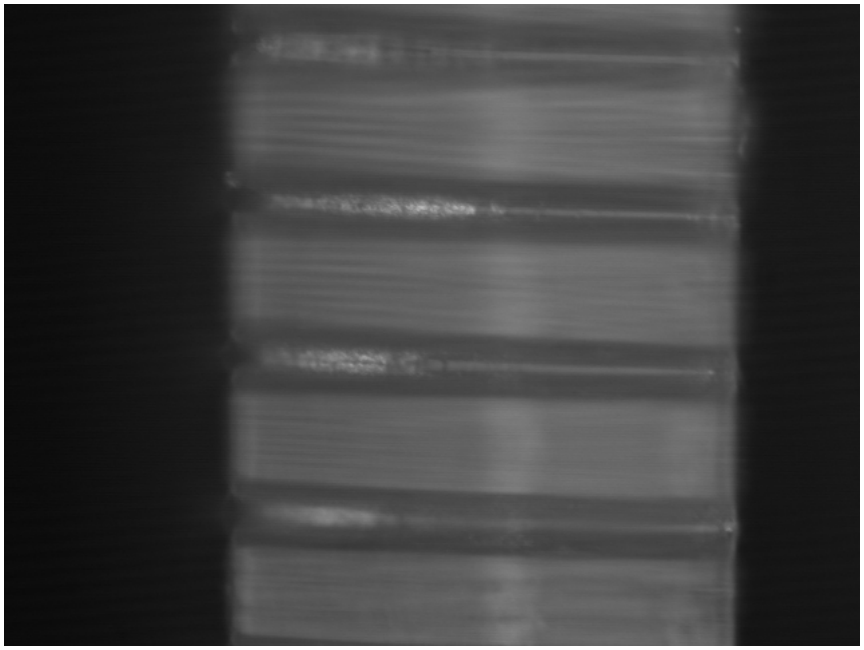

(b)

Fig 34: Developed at 150rpm, room temperature by process shown in 26a. Cross section of a sample cleaved through the comb in 130um thick SU8-50 resist. Gap between the combs shown is 30um and the thickness of the comb is 10um at the 20x magnification. (a) Photographed at 20x magnification. (b) Photographed at 50x magnification.

At a resist thickness of over 100um this development technique was not good enough for the bistable beam development. The beams stop developing after a certain length as shown in figure 36c.

Ultrasonic development was also tried at room temperature in EMDL. The results were not as good as the mechanical stirring.

The substrate was then subjected to a different kind of development technique in the hope of getting better developed bistable beams. The development of the type shown in figure 26b was carried out. The substrate was placed offset in a Petri dish and rotated by 90 degrees 4 times during the course of development. The direction of the flow during rotation was such that it would either be along the length of the bistable beam or along the length of the comb finger (which happens to be two perpendicular directions). This process showed a slight improvement in the bistable beam length but deteriorated the development of the comb fingers when compared to the earlier structures shown in Figures 35 and 36. The rotated sample figures are shown in 37.

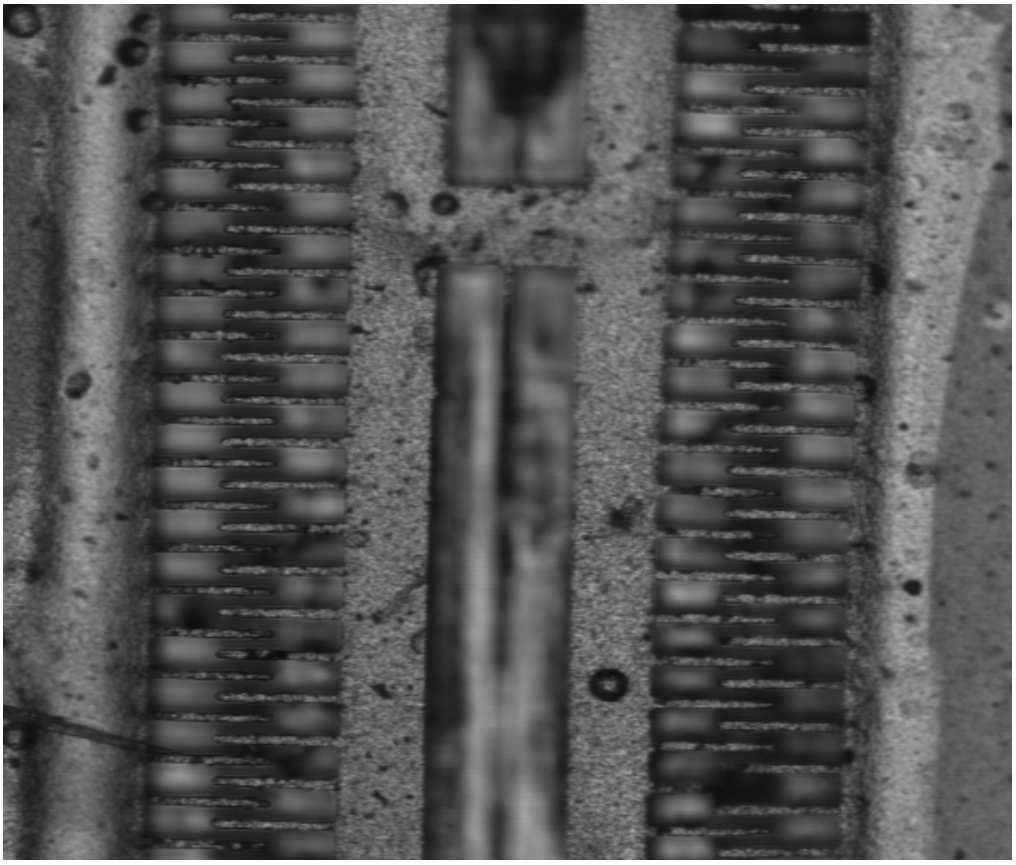

Figure 35: 100 um thick SU8-50 resist developed at 150rpm, room temperature by process shown in 26a.Plated for 30um. Total structure at a magnification of 10x.

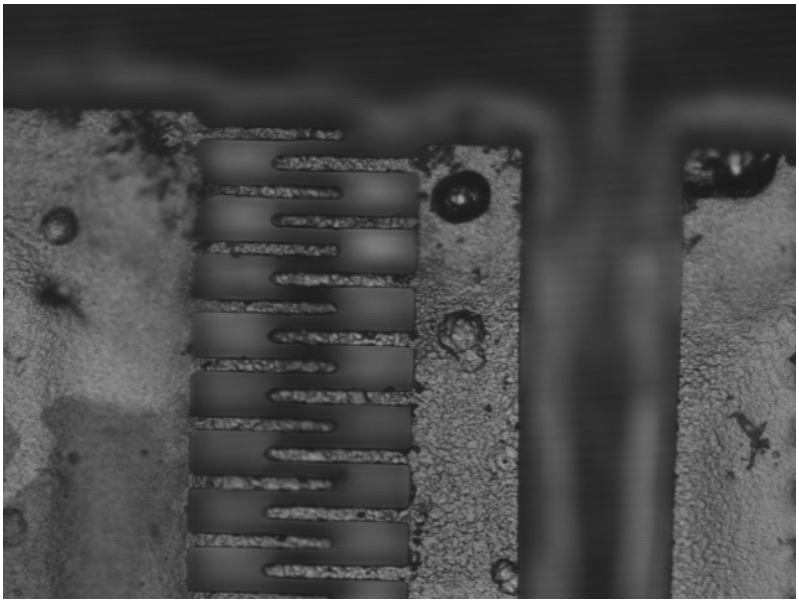

(a)

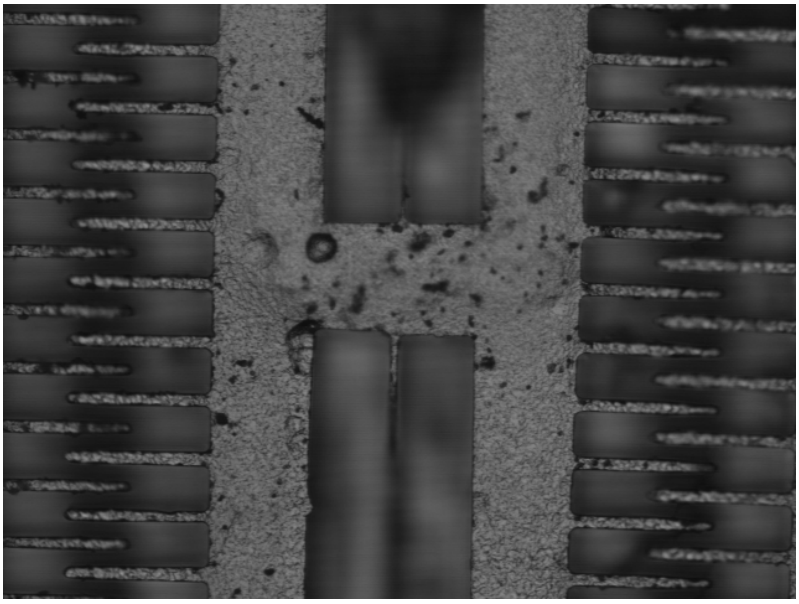

(b)

Fig 36: 100um thick SU8-50 resist developed at 150rpm, room temperature by process shown in 26a. Photographed at 20x magnification. (a) One set of combs 100um long and 10um thick, completely developed and plated. (b) Both set of combs and a part of the bistable beam plated. (c) Bistable beam of thickness 10um stops developing after a length of 200um (figure continued).

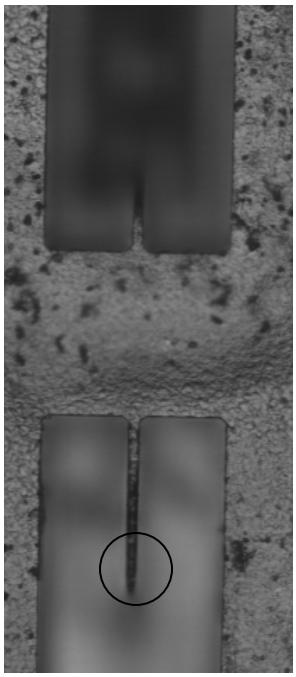

(c)

- **For 40um Thick SU8-50 Resist**

Mechanical stirring at room temperature

The thickness of the resist was reduced to 40um due to incomplete development of the bistable beam length for a resist thickness of over 100um. The development process with mechanical stirring (figure 26a) was attempted once again. The structures were plated 10um tall. The pictures of structure 17 (table2) are shown in figure 38 and 39. There was a significant improvement found in the bistable beam length developed without any deterioration in the development of the combs (as seen earlier). Bistable beam lengths of 850-900um were found developed over the entire length of the beam.

On rotation of the sample by 90 degrees during plating, beam lengths developed were about 600um and the combs were not completely developed (pictures of these are not shown).

Ultrasonic development at room temperature

Ultrasonic development at room temperature was also tried for this 40um tall resist. The results it gave were comparable to the mechanical stirring results but not better. Figure 39 shows images photographed of structure 17 (table 2) having 10um of nickel plating. The development was done in an Ultrasonic bath (Model no: Branson 3500) at CAMD.

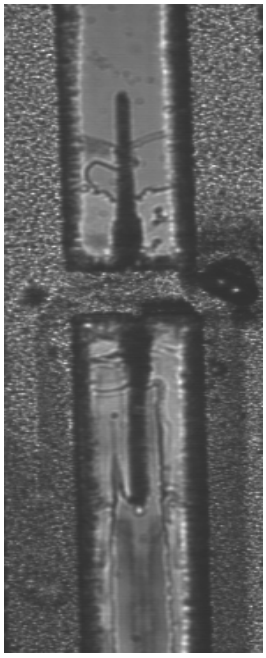

(a)

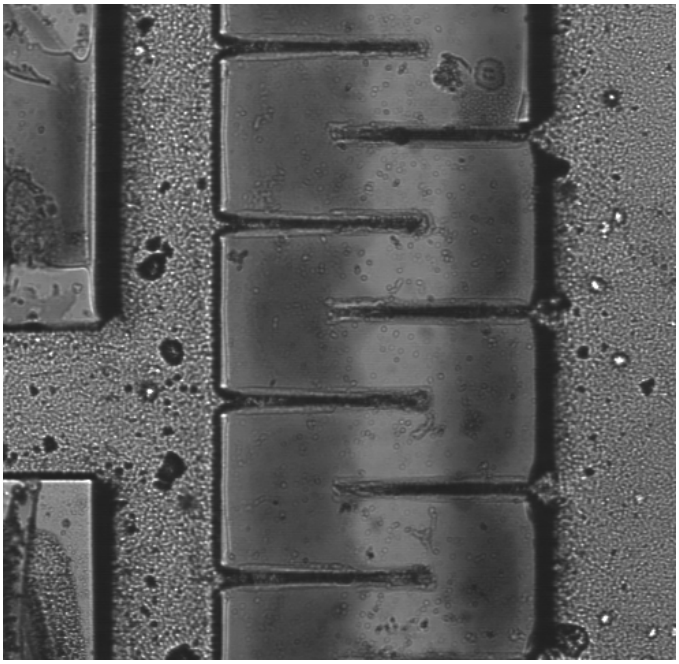

(b)

Fig 37: 100um thick SU8-50 resist developed at 250rpm, room temperature by process shown in 26b. 30um tall plating of samples, structure 11 (Table2) photographed at 20x magnification. (a) Bistable beam plated for 400um over the entire length of the beam. (b) Incomplete development of comb fingers having a gap of 45um and comb length of 120um.

(a)

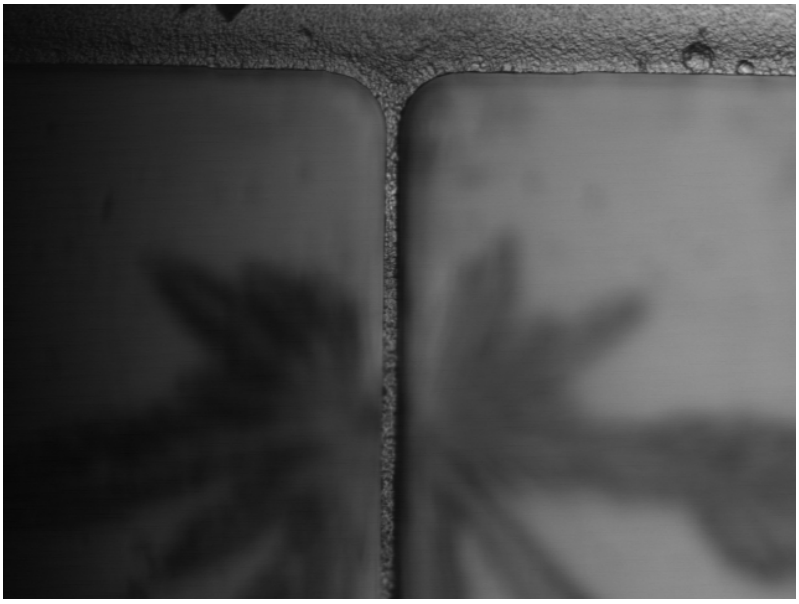

(b)

Fig 38: 40um tall SU8-50 resist developed at 150rpm, room temperature by process shown in 26a. 10um plated samples. The star shape seen under the beam in figures a and b is a defect on the substrate. (a) Bistable beam length of 600um having a thickness of 10um has been developed (photographed at 10x magnification). (b) Bistable beam photographed at 20x magnification. (c) Comb fingers (length of 100um, thickness of 10um, a gap of 15um) and bistable beam around the center with 275um length developed, photographed at 20x magnification (figure continued).

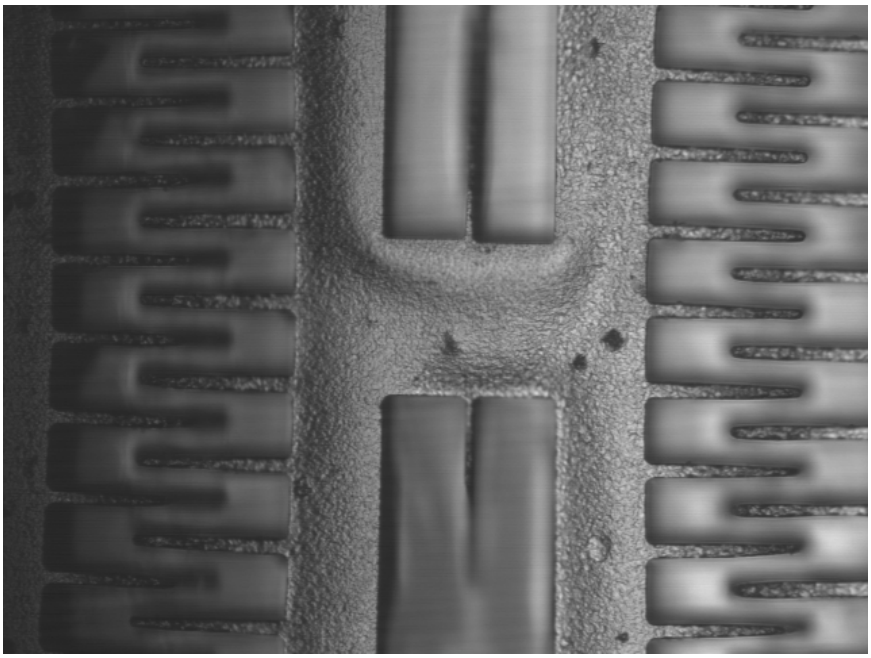

(c)

The sample was held perpendicular to the bottom of the bath on a wafer holder. It was rotated in the same plane 4 times during the course of development.

4.4 Conclusions

The best development results obtained for various resist thicknesses was from the mechanically stirred samples. The maximum bistable beam lengths developed under available lab conditions were less than 1mm (850-900um) for a beam thickness of 10um. The comb finger lengths that were developed ranged from below 100um to 200um for a comb finger thickness of 10um. The minimum gap between the combs needed to ensure proper development was 5um.

For a reasonable amount of compression in bistable beams of length below 1 mm the voltages required are very high (over 500V when computed through the derived design equations). Hence the feasible fabrication dimensions were not practically useful.

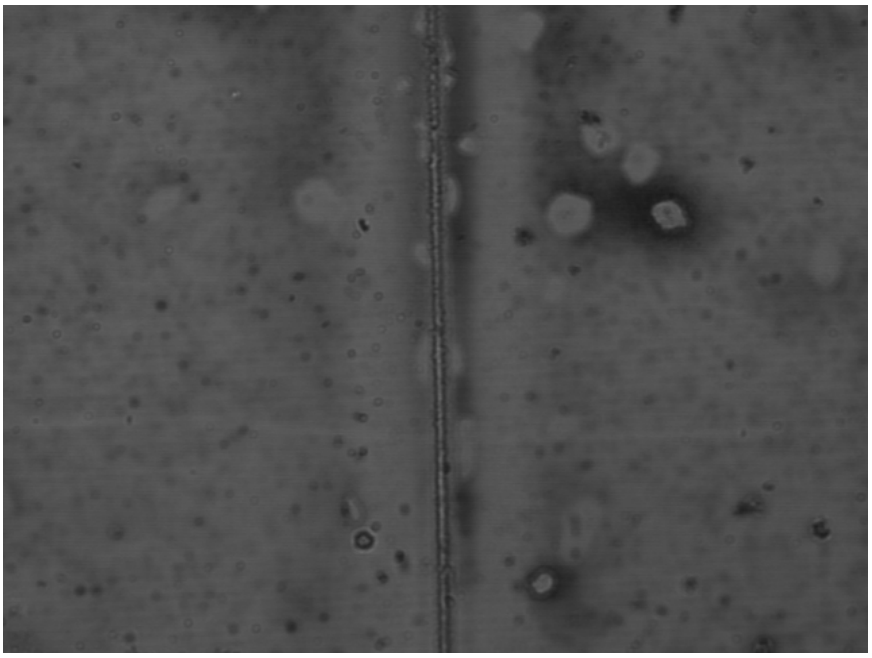

(a)

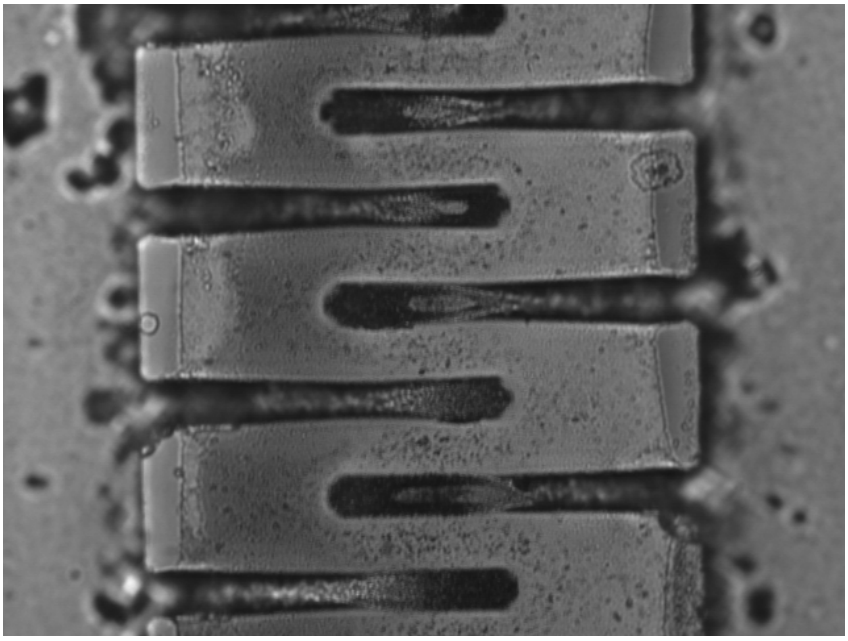

(b)

Fig 39: 40um tall SU8-50 resist developed in an ultrasonic bath at room temperature (at CAMD) (a) Bistable beam length of 600um having thickness 10um (photographed at 20x magnification) (b) Comb fingers of length 100um, thickness 20um and gap12um (photographed at 50x magnification).

The availability of better facilities such as a Mega sonic bath would likely dramatically improve the development of the beams. These facilities are nominally available at CAMD but are currently not operational. SU8-50 resist over 1mm thick has been developed using the mega sonic at room temperature [10]. Though the lengths of the beams developed were small compared to the bistable beams designed, this is still a possibility [11]. Redesigning the structures is also a possibility for improvement but even then atleast beam lengths of 2.5mm are required in order to obtain reasonable compressions and voltages.

Bibliography

1. Pratul K Ajmera and In-Hyouk Song, “Laterally Movable gate FET (LMFET) for on chip integration of MEMS with electronics,” Proc. SPIE Int. Soc. Opt. Eng., p.4334, Vol. 30 (2001)

2. In-Hyouk Song and Pratul K Ajmera, “Use of a photo resist sacrificial layer with SU-8 electroplating mould in MEMS fabrication,” Journal of Micromechanics and Micro engineering (JMM), Vol 13, p.1-6 (2003)

3. Zheng Cui and Ron A Lawes, “A new sacrificial layer process for the fabrication of microelectromechanical systems,” Journal of Micromechanics and Micro engineering (JMM), Vol 7, p.128-130 (1997)

4. Mordechay Schlesinger and Milan Paunovic, “Modern Electroplating”, John Wiley and Sons, Inc., Pg. 13, 15, 141 and 142, 2000.

5. Stefan Stadler and Pratul K Ajmera, “ Integration of LIGA structures with CMOS circuitry”, Sensors and Materials, Vol. 14, No.3, p 151-166 (2002)

6. S.Ramamrutham and R.Narayanan, “ Strength of Materials”, Dhanpat Rai Publishing Company Limited, Pg 226-229, 710-711, 713-714

7. Images obtained from EMDL Website of the Department of Electrical Engineering at Louisiana State University: http://www.ee.lsu.edu/emdl/index.html

8. Images obtained from the Center of Advanced Microstructures and Devices (CAMD) at LSU: http://www.camd.lsu.edu

9. Dr.Pratul K. Ajmera, Department of electrical and Computer Engineering, LSU – Private communication.

10. Dr. Wanjun Wang, Department of Mechanical Engineering, LSU – Private communication.

11. Pictures of “UV lithography technology for SU-8” from the personal web page of Dr. Wanjun Wang, Department of Mechanical Engineering, LSU: http://me.lsu.edu/~wang/Research_files/Research_UV_SU8.htm

Appendix: Copyright Permissions

A.1:

"Varsha Francis" <vfranc1@lsu.edu>
06/07/2005 19:20

To permissions@iop.org
cc
bcc
Subject Permission to use journal information

Hello Sir/Madam,

I am a graduate student in the Department of electrical engineering at Louisiana State University, Baton Rouge, LA. This email is to obtain permission from you for use of some material which was of particular interest to me for my reserach and needs to be used in my thesis report. This is from the paper " Use of a photoresist sacrificial layer with SU-8 electroplating mould in MEMS fabrication" by In-hyouk Song and Pratul K Ajmera published in Volume 13 of JMM, pages 1-6 in 2003. The figure I need to use is Fig 1 (the whole of it). If you could grant me that permission I could carry on with my report writing.I hope I hear from you soon.

Thanking You.

Yours Sincerely,

Varsha Francis

PERMISSION TO REPRODUCE AS REQUESTED IS GIVEN PROVIDED THAT:

(a) the consent of the author(s) is obtained
(b) the source of the material including author/editor, title, date and publisher is acknowledged.

IOP Publishing Limited
Dirac House
Temple Back
BRISTOL 12/7/05

BS1 6BE Date Rights & Permission

A.2:

PERMISSION FORM

Dear Madam, dear Sir,

I am preparing for my thesis report
entitled Development of process techniques for bistable microbeam fabrication.
I am requeting permission to use the material described below

1. Title: Integration of LIGA structures with CMOS circuitry
2. Author(s): Stefan Stadler, Pratul K. Ajmera
3. Journal title: Sensors and Materials (Volume. 14 No. 3)
4. Material to be used: Figure 5
5. Page(s): 161
6. Publisher: MYU TOKYO
7. Year of Publication: 2002

Youre sincerely,

Requested by: Varsha Francis
Louisiana State University,
Baton Rouge, LA, USA

Date: July 15, 2005

Permission granted by:

MYU K.K
1-23-3 SENDAGI BUNKYO-KU
TOKYO 113-0022 JAPAN

Date: July 19, 2005
Sawako Ogawa

Vita

Varsha Francis was born on August 24, 1982, in Hyderabad, India. In June 2003 she graduated with a bachelor's degree in electronics and communications engineering from Osmania University, Hyderabad, India. She furthered her study here at Louisiana State University, Baton Rouge, by doing a master's in electrical and computer engineering under the supervision of Dr. Martin Feldman